Università di Pisa

Scuola di Ingegneria

Dipartimento di Ingegneria dell'Energia, dei Sistemi, del Territorio e delle Costruzioni

---

Corso di Laurea Magistrale in
INGEGNERIA ELETTRICA

The integration of storage in HV grids: optimal use of renewable sources

Candidato:

Laura Fiorini

Relatori:

Prof. Paolo Pelacchi
Prof. Marco Aiello
Prof. Davide Poli

Anno Accademico 2014/2015

To my family

Contents

List of Figures

List of Tables

1

Introduction

1.1 New challenges to electric power systems

The transmission system is a complex and interconnected infrastructure that transfers electric energy from generating power plants to electrical substations, located close to demand centres. Most transmission lines are high-voltage, three-phase alternating current; single phase AC is sometimes used in railways systems, while high-voltage direct current (HVDC) technology is used in submarine power cables, typically longer than 50 km.

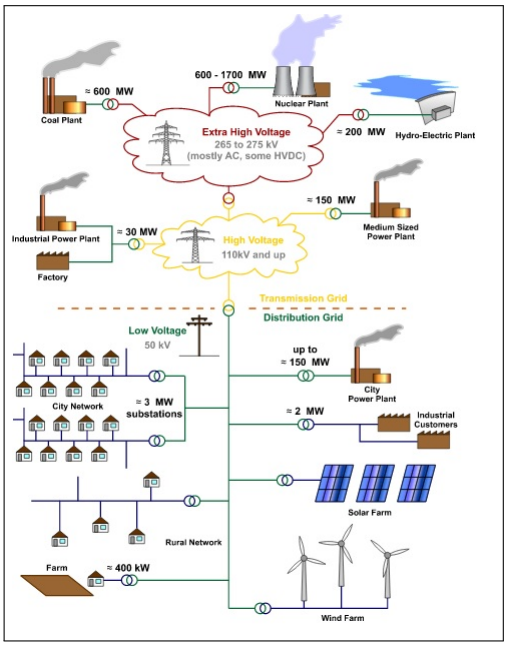

Figure 1.1: General layout of a typical European electricity networks *(Source: Wikipedia)*

According to Joule's law, electricity is transmitted at high voltages, from 110 kV onwards, to reduce the power losses, mostly through overhead power lines, but also underground cables, especially in urban areas and sensitive locations. Since electricity is not a storable product, it is necessary to produce the requested quantity and distribute it through the network in such a way to guarantee that supply and demand are always balanced. This is one of the tasks of the Transmission System Operators (TSOs), entities independent from the other electricity market players, who have also to guarantee the secure and safe operation and maintenance of the main high voltage grids.

In 2008, the European TSOs joint to form the European Network of Transmission System Operators for Electricity, ENTSO-E, "in order to promote the completion and functioning of the internal market in electricity and cross-border trade and to ensure the optimal management, coordinated operation and sound technical evolution of the European electricity transmission network" [31]. One of the aim of ENTSO-E is putting the European energy policy into practice, promoting the adequate development of the interconnected European grid.

Over the past years, indeed, new kinds of generation and exploitation of Renewable Energy Sources (RES) has been encouraged significantly [17], in order to fulfil the 2020 targets, such as the reduction in greenhouse gas emission, improve the EU's energy efficiency and increase the share of renewable energy [29]. In this scenario, the role of TSOs becomes more complex, since they are called to face with a continuously growing amount of variable power plants, that means rapid and less predictable flow changes, keeping the power system's reliability at acceptable levels and progressively removing the obstacles towards an unified European energy market [22]. The network is itself subjected to new operational conditions: power flows don't follow any more the traditional paths from major centres of production to consumption ones, since most of RES plants are linked to the distribution grid or very often far away from consumption sites, e.g. offshore wind farms. The transmission network has to be ready to accommodate bi-directional flows and be flexible.

Anyway, the expansion and planning of energy power systems is a very complex and expensive process, that has to face the strongest public opposition against new overhead lines and long-lasting permit procedures [23]. REALISEGRID is a new EU research project for assessing how the transmission network should be optimally developed to achieve a reliable, sustainable and competitive electricity supply [32].

In this context, different kinds of energy storage systems (e.g. PHS, CAES, FES, SMES, Na-S batteries) could be the key elements for making the renewable production more flexible [26], with two major benefits. On one hand, they can store the excessive energy during the off-peak periods and release it when the load demand is high, reducing the thermal pro-

ductions and, thus, the carbon emission. On the other one, these devices could maximize the stability of the grid and relieve transmission congestion, preventing more expensive solutions, such as generation re-dispatching and start-up of fast unit [1].

1.1.1 Research question

This thesis work is developed with the aim of investigating how the introduction of storage systems can bring benefits for a power system with a high penetration of renewable production.

Our first research question deals with the model of the grid: how can a power system be represented as a graph, taking into account its fundamental physical aspects and the main characteristics of its components?

The second goal is running a DC power flow to minimise an objective function. Given the load demand and the installed generation plants, which is the objective function that minimizes the daily operational costs, maintaining the supply-demand balance?

Finally, we introduce some storage systems. Do they lead a better exploitation of the renewable production, in terms of reduction of curtailment and relief of transmission congestion? Having a set of devices, which is their best siting?

1.1.2 Methodology

This thesis consists in two main parts: the topological representation of a power system as a graph and the simulation of a DC power flow above it. In the first part, the grid used as test case is topologically represented as a weighted graph, by describing four kinds of node and assigning the main line characteristics to the edges; load demand and renewable profiles are defined deterministically over a 24-hour horizon and with a quarterly resolution. Then, a DC power flow is run above all the grid, with the aim of minimizing the daily costs of production. At the beginning, in case of surplus of available renewable power, the model takes into account only the possibility of curtailment, while, at a later stage, some storage systems are added, following different policies.

Both goals are reached by means of a new developed program, which solves a linear programming problem, where the variables involved are subjected to constrains.

1.2 Thesis scope and organization

The scope of this thesis is the evaluation of the introduction of electrochemical storage systems in a HV grid, represented as a graph by a topological

point of view, over a 24-hour horizon, in order to minimize the operational costs.

In Chapter 2 we provide a brief state of the art in the field of complex network analysis applied to power systems and to sizing and siting of energy storage. Moreover, we review the main tools developed over the last 30 years to simulate and analyse power systems.

Chapter 3 gives a briefly description of different energy storage technologies and their possible grid applications.

Chapter 4 provides the necessary power system background, some fundamentals of network theory and a brief overview of the different energy storages technologies. Then, we explain how a power system can be represented as a graph, by defining four kinds of nodes and assigning the main lines properties to the edges, and which policies are adopted for batteries' sizing and siting. Finally, the main metrics are proposed and explained.

In Chapter 5, we define the objective function and all the constrains of the mathematical model.

Chapter 6 briefly describes the developed software, its main sections and how it works.

Chapter 7 describes the modified version of IEEE RTS-96 used in this work as a test case, how the RES plants are added and their production profiles. We explain how the peaks of load demand have been set, according to the typical seasonal Italian load curves.

Since some simulations are run, Chapter 8 summarizes their setup, the software performances and the results. These ones are distinguished in before and after the storage integration, for a clearer evaluation of its effects in terms of better exploitation of RES sources, resolution of lines overloads and transmission congestions, re-distribution of power flows across the grid.

Finally, Chapter 9 discusses and analyses the results and proposes some future works.

The work is concluded with an appendix including more information about the structures of the data input and output.

2

State of the art

2.1 Power systems and network

Given their importance to modern economies and complexity, it is not surprising that power systems have received a lot of attention in the fields of network science and complex system analysis. Several works have been proposed to identify a link between the structure of a network and the risks related to such a network.

Rosas-Casals et al. present in [33] an analysis of the topological structure and tolerance to failures and attacks of the UCTE power grid, that involves thirty-three different networks. They introduce a simple model of the grid, treating identically all its components, and conclude that the planning strategies to extend transmission systems should take into account the relative increase in vulnerability with the size. Chassin and Posse in [9] propose a method for estimating system loss of load probability only based on the topological structure of the grid and they test it on the North American eastern and western electric grids. Crucitti et al. in [11] build the network of the GRTN Italian grid and show that, because of its heterogeneity in the load nodes, it is pretty robust to most failures, but very vulnerable when the failures occur on the nodes with the highest betweenness. Anyway, these and many other studies use pure topological metrics, neglecting the equations that govern a power network. To fill these gaps, Bompard et al. ([2], [6]) combine topological model with DC load flow model and propose new metrics to provide an assessment of the system vulnerability. They extend the complex network approach by considering the distance in terms of impedances of the lines and bringing into the model the concept of line flow limit.

Moreover, the betweenness and efficiency analysis are widely applied to power grid to identify the most critical nodes and lines, based on shortest path concept ([15], [10]). Anyway, there are some problems with these approach, since the power doesn't flow only along the shortest paths, but along

all the available connections from generators to loads. According to the betweenness measure based on network flow defined by Freeman et al in [18], a new centrality index is proposed by Dwivedi et al. in [16]. This parameter is based on the maximum power flowing from generators (sources) to loads (sinks) through the connecting transmission lines (edges). In this way, the links which carry the greater portions of the total flow are identified as the most important.

In our work, a modified version of the IEEE Reliability Test System 1996 is used as a test case. Parameters such as phase angle and reactance are included to achieve accurate results from the DC load flow, and the nodes are distinguished in generators, loads and storages by assigning different properties. We rank the most exploited lines by defining an Utilization index , in order to determine what percentage of the line's capacity is used, and we provide a centrality analysis, based on the index proposed in [16].

2.2 Sizing and siting of storage systems

The literature in the fields of storage systems for power grid can be divided into three groups: operation, sizing and siting. Most papers focus on the first aspect, that is, given a device with energy and power capacities already defined, they try to maximize the expected operational profit. In [4], for example, two strategies are compared, i.e., the energy is released as soon as the local network can absorb it, or the energy is stored until the price of electricity is higher. Moreover, they seldom take into account the transmission network constraints, e.g. in [21].

Papers regarding the sizing problem often aim to find the optimal capacity at a fixed location, usually close to a wind farm or a large load. Chakraborty et al. in [8] approach this topic by reducing the total operational costs of two power systems, with different number of thermal units and associated costs. In [42], a battery is incorporated into a power buffer for a wind farm, and the capacity is determined with the purpose of keeping the injected power from the farm at a constant level. A novel prospective is presented by Makarov et al. in [25], where, using discrete Fourier transform to decompose the required balancing power into different periodic components, the optimal sizing of storage systems is determined in the time horizons over which they are most effective, according to their technologies.

The siting problem is often connected with the previous one. Dvijotham et al.[14] develop a heuristic algorithm, which places storage at all buses with an unlimited power and energy capacities and then solves an optimization problem to restrict the number of devices, based on their activity at each node, over a large range of realizations of wind fluctuations. In [30], assuming a vertically integrated utility, Pandzic et al. consider both the economic and technical aspects of the problem, by minimizing the sum of the

generation costs and the daily investment cost in storage over a whole year. In a first step, storage is available in any capacity at any node, then the best locations are identified, according to the benefits that distributed storage units can perform, and finally their optimal size is determined averaging over a year the daily maxima of stored energy and injected or extracted power. Del Rosso and Eckroad have an entirely different approach in [12], where they investigate the use of storage to increase transmission capability of congested transmission network. In their work, they prove this concept by adding batteries of various sizes in a critical point, identified through a sensitivity analysis.

In this thesis, we add a set of batteries whose size is determined according to the capacity of the connected lines, then we change their locations by following three different policies, in order to investigate their possible effects on the grid in terms of reduction of curtailment and relief of overloads and congestions.

2.3 PSA tools

Power System Analyzers (PSAs) are simulation tools need to create accurate replicate of all the physical events that can occur in a network. The more complex and complicated are the grids, the more powerful and advanced tools are required. PSAs can be divided in two groups: commercial and educational/research-aimed softwares.

Commercial softwares are complete and computationally efficient, but also "closed", i.e. they can't be modified. For research purposes, the flexibility and the possibility of making changes are often the most important aspects [27]. There is a large variety of open sources tools [3], and Matlab is the most common choice, which offers a graphical environment (Simulink) that enables user to perform interactive tasks. Many Matlab-based power systems tools have been proposed, such as Power System Toolbox (PST), MatPower, Voltage Stability Toolbox (VST), MatEMTP, SimPowerSystems (SPS), Power Analysis Toolbox (PAT), and the Educational Simulation Tool (EST). Among these, only MatPower and VST are open source [27]. These packages can solve many different typical problems, such as power flow (PF), continuation power flow (CPF), optimal power flow (OPF), small-signal stability analysis (SSA) and time-domain simulation (TD).

The software developed in [41] and used in this thesis can be collocated among the research-aimed PSA and it aims to achieve an optimal power flow with a linear programming approach, focusing on the problems deriving from the penetration of renewable sources and storage into power systems.

3

Energy storage systems: a brief overview

European de-carbonisation energy policy has significantly increased the production from Renewable Energy Sources (RES) over the past years [17]. In Italy, in 2012 electricity production from RES totalled 93 TWh/y: 45.4% came from hydro sources, 14.5% from wind, 20.5% from photovoltaic, 6.1% from geothermal and 13.5% from bioenergy [39]. In this situation, the network is subjected to new operational conditions. Power flows don't follow any more the traditional paths from major centres of production to consumption ones, since most of RES plants are connected to the distribution grid. Moreover, wind and solar are intermittent and volatile, thus resulting in a varying power supply. For these reasons, the transmission network has to be ready to accommodate bi-directional flows and to be more flexible than in the past. Two options are included into the model to improve system flexibility: renewable power curtailment and energy storage.

3.1 Renewable power curtailment

Renewable power curtailment can be used to reduce the amount of RES power injected into the network. Wind and solar have zero or very low marginal costs, which means that as long as all transmission and operating constraints are met, wind and solar tend to substitute thermal generation. However, there are many reasons for using less wind or solar power than potentially available at a certain time, e.g. transmission congestions and minimum technical power output of thermal generators [24].

Curtailment of production should be managed according to a least-cost principles in a system prospective. Since renewable power is almost free, its restriction should be the least solution.

3.2 Main characteristics of EESS

Electric energy storage systems (EESS) store the electric energy in a kinetic, potential, electromagnetic or electrochemical form which can be converted back to the electric one when required. The most important functional characteristics of energy storage for transmission system application are summarized here above [12], [7].

- *Energy capacity*: the energy quantity that can be stored.
- *Power capacity*: the rate at which the amount of energy flows in and out of the storage system.
- *Response time*: how quickly a storage technology can respond when it's commissioned.
- *Discharge duration*: how long a device can maintain output. The ratio between energy and power capacity gives the discharge duration at maximum power level.
- *Efficiency*: the round-trip ratio between absorbed and provided energy. For all the storage systems, energy is lost in the process of charge and discharge, but also while the device is not used (stand-by losses).
- *Depth of discharge* (DoD): the ratio between stored energy and rated energy capacity, at a given operational condition. Deep discharge of some electrochemical batteries reduce their life and may ruin them.
- *Life*: after how many charge-discharge cycles the storage needs to be replaced. Strongly affected by DoD.

3.3 EES technologies

There are several energy storage technologies that serve different applications depending on the amount of energy to be stored, the rate at which it must be transferred and the response time, e.g. pumped hydro storage, battery, compressed air energy storage (CAES), flywheel, superconducting magnetic energy storage (SMES), capacitors.

Pumped hydro storage At present, this technology is the most important means of electricity storage, with over 100 GW in operation worldwide ($\sim$32 GW installed in Europe, $\sim$21 GW in Japan, $\sim$19.5 GW in the USA and other in Asia and Latin America [10]).

The principle is well known: during off-peak periods, the electricity is stored as potential energy by pumping water to a upper reservoir. When

demand is very high, the water flows from the upper to the lower reservoir and activates the turbines to generate high-value electricity.

PHS is a mature technology, with a conversion efficiency of about 65-80%, depending on equipment characteristics [20].

Compressed air energy storage CAES uses electrical power during off-peak hours to compress air at high pressure (40-70 bars) and store it in underground reservoir; during peak hours, the air is drawn from the storage vessel, heated in a combustion chamber and expanded first in a high pressure turbine and then in a low pressure one. Both turbines are connected to a generator to produce electricity. Since this technology uses fuel, it is also known as hybrid energy storage.

CAES has a relatively long storage period, low capital costs and high efficiency [10].

Flywheel A flywheel stores energy in the form of kinetic energy of a rotor spinning around a shaft. On one hand, this technology has a great cycling capacity (from 10 000 to 100 000 cycles); on the other one, high friction losses and decreasing efficiency in time (from 85%, to 78% after 5h and% after one day, considering losses at about 200kW for a 200 tons flywheel) make long-term storage not foreseeable [20].

Superconducting magnetic energy storage SMES stores electricity as a magnetic field created by the flow of electric current through an inductor made of superconducting material at very low temperature (-269° C). This technology offers a very high efficiency ($\sim$97% in very large systems) and rapid response, but the major negative aspects are the high costs and environmental issues related to the strong magnetic fields [10].

Capacitors Electrochemical capacitors consist of two electrodes, a dielectric and two current collectors. Within these devices, charge is stored electrostatically and energy is directly related to the surface area of the electrode and the square of the voltage applied across the terminals.

Supercapacitors have generally a durability of 8-10 years, an efficiency of 95%, but also a high energy dissipation rate of 5-40% per day, which means that the stored energy must be used quickly [20], [5].

Battery A battery is composed of several electrochemical cells, connected in series and/or parallel with the aim to provide the required voltage and capacity, respectively. Each cell consists of two electrodes, where the redox reactions take place, and an electrolyte solution, usually containing dissociated salts to transfer ion between the two electrodes. Once these ones are

connected externally, the chemical reaction proceed at both of them, thus liberating electrons and providing the current for the user [13].

The most common technology commercially available for permanent applications are [40]:

- Lithium Ion, based on Li-ions intercalation compounds. Li ions migrate across the electrolyte between the two structures, which serve as anode and cathode. This batteries enable high-output voltages, high-energy density and long cycle life [13]. A storage system with power capacity up to around 1 MW can be totally containerized.

- Flow battery, whose basic cell consists of two electrolyte flow compartments separated by an ion-selective membrane. The energy is stored in the electrolyte itself and individual cells are arranged in stacks by using bipolar electrodes [13].

- Sodium sulphur, that is a high-temperature technology using β-allumina solid electrolyte tube containing molten Na (negative electrode) and surrounding by molten S (positive electrode). The high temperature (270-350° C) is required in order to take advantage from the increased conductivity of the β-alumina and ensure the molten state of the electrode materials [13].

- Sodium nickel chloride, better known as ZEBRA (Zero- Emission Battery Research Activities). The two electrode are physically and electrically divided by a β-allumina ceramic separator, which is also the electrolyte. The negative electrode is molten Na, while the positive one is a semi-solid combination of $NiCl_2$ and a molten secondary electrolyte, $NaAlCl_4$, therefore a high temperature is required as in the Sodium sulphur technology [13].

3.4 Applications for energy storage

Generally two kinds of energy storage systems applications can be distinguished: energy intensive and power intensive. The former is available to store large amounts of energy, while the latter delivers and absorbs great amount of power in short time. Fig.3.1 shows the characteristics for several EES systems in terms of power rating and duration of discharge.

Potential grid applications range from peak shaving and load shifting, which can foster improvements in grid capacity and cost, to voltage and frequency regulation, for a better power quality.

Energy intensive applications are mainly oriented towards the shifting of energy flows over time. Valuable energy (e.g. from wind and solar farms) can be stored during off-peak periods, for example at night when

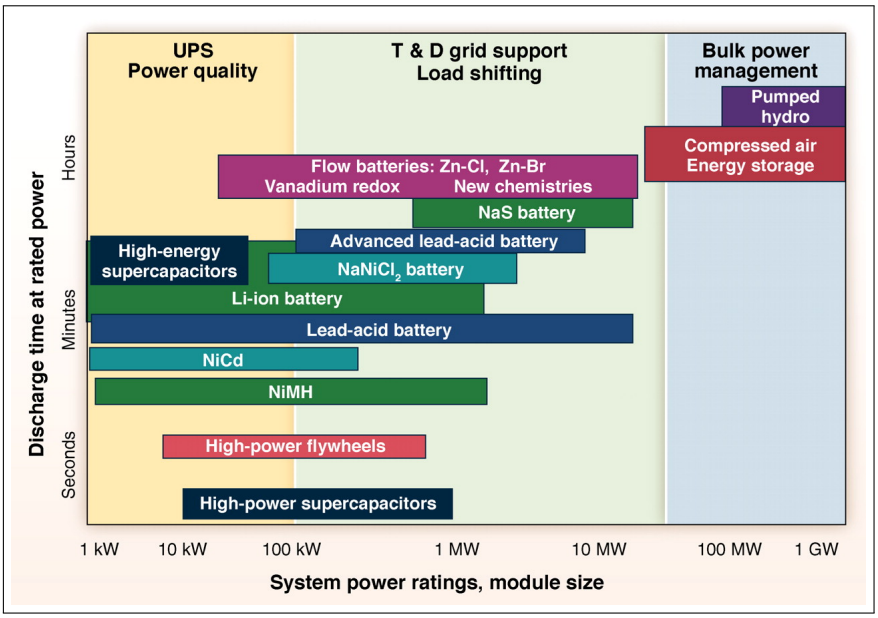

Figure 3.1: Comparison of discharge time and power rating for various EES technologies *(Source: EPRI)*

the load demand is low, and then used at peak times, thus increasing the penetration of renewable energy into the power grid and reducing the gap between daytime and night-time, that may allow conventional generation production to become flatter, which contributes to an improvement in operating efficiency and fuel cost reduction [36]. In addition, when a critical line is overloaded, the wind production has to be curtailed in order to solve the problem. This can be mitigated by using large energy storage, until the operator can find a permanent solution.

Power intensive applications respond quickly to requests for high amounts of power in short periods (e.g. few seconds or minutes) for several purposes, such as frequency regulation, voltage control and substitutive reserve, in order to guarantee grid stability and power quality.

In this work, we take into account only battery storage systems, without any distinction between different technologies, dimensioned for energy intensive applications.

4

Power system as a network

4.1 Linearized power systems model

[1] Transmission lines can't transfer power flow with perfect efficiency, that is the power delivered at the receiving-end of the line is generally less than the power sent from the sending-end, due to losses in the line resistance. This is determined by materials and design parameters of the lines, such as length, diameter and line spacing. Since power transmission systems operate in a sinusoidal steady state, it is necessary to introduce the concept of *impedance* $\overline{Z}$, that extends the concept of resistance to AC circuits, by taking into account two additional mechanisms, i.e. inductance and capacitance. For this reason, the complex impedance can be defined as the measure of the opposition that the line presents to a current flow when a voltage is applied and it is constructed with the real component expressing resistance R and the imaginary one expressing the reactance X.

$$\overline{Z} = R + jX \tag{4.1}$$

The resistance determines the electrical losses, while the reactance measures the strength of the line's magnetic field due to a current flow through the line. The higher the impedance, the smaller is the current, for the same applied voltage. We can also define a complementary property to measure how easily current flows across a connection. The admittance of the line is:

$$\overline{Y} = \overline{Z}^{-1} = G + jB \tag{4.2}$$

where $G = \frac{R}{R^2+X^2}$ is the conductance and $B = -\frac{X}{R^2+X^2}$ the susceptance of the line. For a circuit made of N buses operating in AC regime, the nodal

[1] For this section, we refer mostly to [2].

equations can be written as follows:

$$\begin{pmatrix} \overline{I_1} \\ \overline{I_2} \\ \vdots \\ \overline{I_N} \end{pmatrix} = \begin{pmatrix} \overline{Y_{11}} & \overline{Y_{12}} & \cdots & \overline{Y_{1N}} \\ \overline{Y_{21}} & \overline{Y_{22}} & \cdots & \overline{Y_{2N}} \\ \vdots & \vdots & \ddots & \vdots \\ \overline{Y_{N1}} & \overline{Y_{N2}} & \cdots & \overline{Y_{NN}} \end{pmatrix} \begin{pmatrix} \overline{V_1} \\ \overline{V_2} \\ \vdots \\ \overline{V_N} \end{pmatrix} \tag{4.3}$$

where

$$\overline{I_i} = I_i e^{j\delta_i} \quad \overline{Y_{ij}} = Y_{ij} e^{j\gamma_{ij}} \quad \overline{V_i} = V_i e^{j\theta_i}$$

are the phasors representing the sinusoidal functions of currents, admittances and voltages. A phasor $Ae^{j\omega t}e^{j\theta}$ is a complex number with a time-invariant amplitude (A), frequency (ω) and phase (θ). In an isofrequential circuit, the shorthand notation $Ae^{j\theta}$ can be used and $f = \frac{\omega}{2\pi}$ is the circuit's frequency. In matrix notations, Eq.(4.3) is:

$$\mathbf{I} = \mathbf{YV} \tag{4.4}$$

where $\mathbf{I}$ is the vector of current sources, $\mathbf{Y}$ is the line admittance matrix and $\mathbf{V}$ is the vector of node voltages. The elements of $\mathbf{Y}$ are calculated as follows:

- diagonal elements $\overline{Y_{ii}}$: sum of the admittances of all the lines connected to node i
- off-diagonal elements $\overline{Y_{ij}}$: minus the admittances of the line connecting nodes i and j. It is zero if there is no physical connection between i and j.

The complex power $\overline{S}_i$ that flows through a node i is defined as the product of voltage $\overline{V}_i$ and the conjugate of current $\overline{I}_i$:

$$\overline{S}_i = \overline{V}_i \overline{I}_i^* = \overline{V}_i \sum_{k=0}^{N} \overline{V}_i^* \overline{Y}_{ik}^* = P_i + jQ_i \tag{4.5}$$

where P and Q are called respectively *real* and *reactive* power. The quantities involved in a AC system have a sinusoidal waveform, thus solving a full AC power flow model means solving a system of non linear equations for each node i.

$$\begin{cases} P_i = \sum_{j=1}^{N} |Y_{ij} V_i V_j| \cos(\theta_i - \theta_j - \gamma_{ij}) & \text{(4.6a)} \\ Q_i = \sum_{j=1}^{N} |Y_{ij} V_i V_j| \sin(\theta_i - \theta_j - \gamma_{ij}) & \text{(4.6b)} \end{cases}$$

With the following assumptions, the AC power flow problem can be reduced to a set of linear equations known as *DC power flow*:

- all voltages magnitudes are normalized to 1 per unit
- line losses are ignored, that is the resistance of each line is neglected. Only the reactance x in pu is considered. This assumption is justified by the fact that resistances of transmission lines are often at least an order of magnitude smaller than reactances;
- $\gamma_{ij} = \frac{\pi}{2}$;
- all voltage angles are assumed to be close to each other, that is:

$$\theta_i \approx \theta_j \Rightarrow sin(\theta_i - \theta_j) \approx (\theta_i - \theta_j)$$

- reactive power flows are ignored.

According to these assumptions, the power flow through the line connecting nodes i and j, is given by:

$$f_{ij} = P_i = -P_j = \frac{v_i v_j sin(\theta_i - \theta_j)}{x_{ij}} = \frac{\theta_i - \theta_j}{x_{ij}} \tag{4.7}$$

where v_i and v_j are the node voltage in p.u.

In a circuit with N node and L lines, where $\overline{P}$ is the vector of power injections, which is the local generation less the local demand, $\overline{\theta}$ the vector of phase angles and $\overline{f}$ the vector of power flows, we have:

$$P_i = \sum_{j \in \Gamma(i)} f_{ij} = \sum_{j \in \Gamma(i)} \frac{\theta_i - \theta_j}{x_{ij}} \tag{4.8}$$

$$\overline{P} = B\overline{\theta} \tag{4.9}$$

where B is the $N \times N$ admittance matrix:

$$B_{ij} = -\frac{1}{x_{ij}} = b_{ij} \quad \text{for } i \neq j \tag{4.10}$$

$$B_{ii} = \sum_{j \neq i} \frac{1}{x_{ij}} = -\sum_{j \neq i} b_{ij} \tag{4.11}$$

where b_{ij} is the susceptance of the line between nodes i and j.

In terms of vector of flows f:

$$\overline{f} = H\overline{\theta} \tag{4.12}$$

where H is the $L \times N$ transmission matrix:

$$H_{li} = -H_{lj} = \frac{1}{x_{ij}} = -b_{ij} \tag{4.13}$$

$$H_{lk} = 0 \quad \forall k \neq i, j \tag{4.14}$$

The system of equations given by Eq.(4.9) generates N equations with N unknown bus voltage angles θ. Since these equation are not independent, the system is not identified. For this reason, the voltage angle at one bus, for instance node N, is set to zero $\theta_N = 0$. This bus is referred to as the *slack node*. In this way, one of the equations in the system becomes unnecessary and we get an independent one of N-1 equations $\overline{P}'$ with N-1 unknowns $\overline{\theta}'$, without the node N. By deleting the row and the column corresponding to the slack node in matrix B and H (in this case, only the column), we obtain the matrix B' that has an inverse B'^{-1} and H'. According to this:

$$\overline{\theta}' = B'^{-1}\overline{P}' \tag{4.15}$$

$$\overline{f} = H'\overline{\theta}' \tag{4.16}$$

According to the above explanation, the larger the difference between nodal voltage angles, the greater power flow along that line. Once the vector $\overline{\theta}$ is known, we can determine the vector of flows $\overline{f}$ above all the grid.

In this work, the vector $\overline{f}$ is expressed in terms of (MW), that is, each flow is defined as in Eq.(4.7) multiplied by the base power P_b of 100 MW, since all pu quantities of the test system used as case study are on this base value.

4.2 Fundamentals of network theory

As a preliminary step, let us briefly recall some definitions and concepts from the network theory.

Definition 4.1 (**Network).** A *Network* is, in its simplest form, a collection of points joined together in pairs by lines. The points are referred to as vertices or nodes and the lines are referred to as edges [28]. The vertices belonging to an edge are called *end-vertices* or *end-points* of the edge.

Definition 4.2 (**Power grid graph).** A *Power grid graph* is a pair (V, E) such that each element $v_i \in V$ is either a substation, transformer, or consuming unit of a physical power grid. There is an edge $e_{i,j} = (v_i, v_j)$ with $e_{i,j} \in E$ between two nodes if there is a physical cable connecting directly the elements represented by v_i and v_j.

There are two kinds of graphs or networks, *directed* and *undirected*.

Definition 4.3 (**Directed graph).** A *directed graph*, also called a *digraph* for short, is a network in which each edge has a direction, pointing from one vertex to another. Such edges are themselves called directed edges, and can be represented by lines with arrows on them [28].

In this kind of networks, data flow in only one direction of the connecting edge.

Definition 4.4 (**Undirected graph).** An *undirected graph* is a network in which each edge has no orientation, i.e.

$$\forall(v_i, v_j) \text{ if } (v_i, v_j) \in E \text{ then } (v_j, v_i) \in E$$

Definition 4.5 (**Adjacency and Neighbourhood).** If $e_{x,y} \in E$ is an edge in the graph G, then x and y are *adjacent* or *neighbouring* vertices and the vertices x and y are *incident* with the edge $e_{x,y}$. Two vertices are *adjacent* if they have exactly one common end-vertex. The set of all vertices adjacent to a vertex $x \in V$, called the *neighbourhood of* x, is denoted by $\Gamma(x)$.

Every edge $(v_i, v_j) \in E$ has a non-negative, real-valued capacity $c(v_i, v_j)$. If $(v_i, v_j) \notin E$, we assume $c(v_i, v_j) = 0$.

Definition 4.6 (**Flow).** A *Flow* over a graph is a real function $f : V \times V \to \mathbb{R}$ such that:

$$-c(u, v) \leq f(u, v) \leq c(u, v) \tag{4.17a}$$

$$f(u, v) = -f(v, u) \tag{4.17b}$$

$$\sum_{(u,v)\in E} f(u, v) = \sum_{(v,z)\in E} f(v, z) \tag{4.17c}$$

for each vertex $v \in V$.

Going into detail:
(4.17a) *Capacity Constraint*: the flow can't exceed the capacity of the edge.
(4.17b) *Skew symmetry*: the flow from u to v must be opposite to the flow from v to u.
(4.17c)*Flow conservation*: the net flow to a node is zero, except for sources, which "produce" flow, and sinks, which"consume" flow.

4.3 Centrality index and utilization index

In the graph theory, an important property is the distance between two nodes, in particular the minimal one, called *shortest path* or *geodesic distance*.

Definition 4.7 (**Path and path length).** A *Path* of G is a subgraph P of the form:

$$V(P) = \{v_0, v_1, \ldots, v_l\}, \quad E(P) = \{(v_0, v_1), (v_1, v_2), \ldots, (v_{l-1}, v_l)\}$$

such that $V(P) \subseteq V$ and $E(P) \subseteq E$. The vertices v_0 and v_l are the *end-vertices* of P and $l = |E(P)|$ is the *length* of P, that is the number of edges that the path P contains.

Definition 4.8 (**Shortest path).** Given a graph G, the *Shortest path* from v_i to v_j is the path corresponding to the minimum of the set $\{|P_1|, |P_2|, \ldots, |P_k|\}$ containing the lengths of all paths for which v_i and v_j are the end-vertexes.

The concept of *betweenness* is useful to describe the importance of a node or an edge with respect to minimal paths.

Definition 4.9 (**Betweenness of a vertex).** The *betweenness* $C_b(v)$ of a vertex $v \in V$ is

$$C_b(v) = \sum_{v \neq s \neq t} \frac{\sigma_{st}(v)}{\sigma_{st}} \tag{4.18}$$

where σ_{st} is the total number of shortest paths from node s to node t and $\sigma_{st}(v)$ is the number of those paths that pass through vertex v.

Definition 4.10 (**Betweenness of an edge).** The *betweenness* $C_b(e)$ of an edge $e \in E$ is

$$C_b(e) = \sum_{s,t} \frac{\sigma_{st}(e)}{\sigma_{st}} \tag{4.19}$$

where σ_{st} is the total number of shortest paths from node s to node t and $\sigma_{st}(e)$ is the number of those paths that pass through edge e.

Vertices and edges that occur on many shortest paths between any given vertices pair have higher betweenness than those that do not; they have relatively higher importance within the graph.

The measures of betweenness, however, are based on the assumption that information (or power) flows only along the shortest paths, while in a power network it is not true.

According to [18], a new flow-based centrality index is proposed in [16].

Definition 4.11 (**Flow-based centrality index).** Let f_{max} be the maximum flow from the node u to the node v and let f_e be the portion of maximum flow passing through the edge $e \in E$ of the network. The *Flow-based centrality index* $C_f(e)$ is defined as:

$$C_f(e) = \sum_{u \in S} \sum_{v \in T} f_e \tag{4.20}$$

and, by dividing it by the total flow between all pairs of node, the above equation is normalized and expressed in percentage:

$$\widehat{C_f}(e) = \sum_{u \in S} \sum_{v \in T} \frac{f_e}{f_{max}} \cdot 100 \tag{4.21}$$

Moreover, an *Utilizazion index* is defined in order to determine what percentage of the line's capacity is used.

Definition 4.12 (Utilization index). Let f_e be the flow passing through the edge e and let c_e be its capacity, the *Utilization index* $U(e)$ is defined as:

$$U(e) = \frac{f_e}{c_e} \cdot 100 \tag{4.22}$$

and it is expressed as a percentage of the line's capacity.

In this way, the edges can be ranked according to the portion of flow that they carry using Eq.(4.21) or to how much they are exploited using Eq.(4.22).

4.4 Topological representation of power systems

Any network modelled as above (Def.4.2) is symmetric, that means it is an undirected graph [16]. Chassin and Posse have discussed in [9] that a power system can be considered as a directed network in any steady state. Moreover, one can associate a weight to the edge representing a physical line property (e.g. resistance, reactance), so that the system can be evaluated as a weighted graph as defined below.

Definition 4.13 (Weighted Power Grid graph). A *Weighted Power Grid graph* is a Power Grid Graph graph $G_w(V, E)$ with an additional function $w : E \to \mathbb{R}$ associating a real number to an edge representing a physical property of the physical cable represented by the edge, that is the reactance of the line, taken in per unit (p.u.).

4.4.1 Nodes

For the current study, there are four kinds of nodes:

- generators $s_i \in S$ with $S \subset V$, that is the sources set;
- distribution substations $t_i \in T$ with $T \subset V$, that is the sinks set;
- storage systems $b_i \in B$ with $B \subset V$, that is the storage set; and
- bus bars $n_i \in N$ with $N = V \setminus (S \cup T \cup B)$, that is the inner nodes set.

The angle phase θ is a property assigned to all nodes.

Source nodes

The sources are partitioned in *renewable* and *conventional*; only "non-programmable" sources are included in the former type, i.e., wind and photovoltaic. Two subsets of S are defined as follows:

$R = \{r : r \text{ is a renewable energy source RES}\}, \quad P = \{p : p \text{ is a conventional source}\}$

such that $R \cup P = S$ and $R \cap P = 0$.

Generators inject power that has to be transmitted through the edges to the distribution substations.

Sink nodes

The load buses are sinks: they have only incoming flows and their power demand has always to be satisfied.

Storage nodes

These nodes represent the energy storage systems, therefore can have both incoming and outgoing flows. In the first case, they behave as a device in charge, in the second one in discharge.

Inner nodes

The set of inner nodes is defined as follows:

- Each bus from whom more than two lines originate is labelled as an inner node $n \in N$ and the incident edges are weighted in respect of line reactance.
- Each bus from whom one or more lines originate and where a power generation plant (and/or a load and/or a storage) is linked, is modelled as an inner node $n \in N$ with two different kinds of edges incident to it.

4.4.2 Edges

The edges are distinguished in "real" and "dummy".

The "real" edges represent physical transmission lines, they are weighted in respect of the line reactance in pu and their capacity is set equal to the line's one.

The "dummy" ones, instead, are added to connect a source node (or a sink or a storage) to an inner one; a conventional weight of 10^{-4} is given. The capacity of these edges is chosen great enough to drain out the upper power generation limit of the plant or to satisfy the power demand from the load.

4.5 Sizing and siting of batteries

4.5.1 Sizing

The size of each storage added to the grid is determined by the capacity of the line it is connected to. The energy capacity of the battery, indeed, is set

in order to be sufficient to store energy for one hour at the maximum flow allowed on the selected line. Anyway, the last one is significantly greater than the real rate of charge and discharge, since a discharge duration must be taken into account.

This implies that when the line (u, v) has a capacity of $c(u, v)$ (MW), the added storage has an energy capacity equal to $c(u, v)$ (MWh) and a power capacity equal to $\frac{c(u,v)}{K}$ (MW), considering a discharge duration K (h).

We add as many devices as are the lines whose capacities are saturated by a wind farm.

4.5.2 Siting

An utilization index-based analysis helps to identify the most critical lines of the network during the day.

For each line, all power flows during one day can be ordered in descending order to obtain a *power-flow duration curve*. This curve shows how long the power flowing on that line is above a given level. The highest flow experienced during the day, regardless the quarterly this flow occurred on, is represented by the left-most value on the graph.

An analogous curve is obtained by ordering in the same way all utilization indexes, thereby getting an *overload duration curve*.

In this way, the most overloaded lines can be identified and classified in a ranking with the aim of choosing the best location for the storage systems.

Given one of the seven scenarios described in Sec.7.3, we sum the number of quarters of an hour in which a line is loaded up to the 100% of its capacity on all days; then, the average is calculated over all the cases; since four days are taken into account, the maximum value that this parameter may obtain is 384. The ranking is compiled according to this average.

The lines can be distinguished between those linked to a wind farm and those that are not. The storage systems are located by following three different policies:

- choosing a number of buses connected to the most overloaded lines only among the ones linked to a wind farm;
- choosing the same number of buses connected to the most overloaded lines among all the grid; and
- mixing the previous policies, choosing the same number of buses in a random way.

5

Mathematical formulation

5.1 HV grid components in a graph

The next step is adding attributes to the nodes considering the main characteristics of grid components.

5.1.1 Generation plants

Each plant s has upper $P_{s,max}$ and lower $P_{s,min}$ power generation limits which can't be violated, depending on the technology, so that, $\forall s \in S$:

$$P_{s,min} \leq P_s \leq P_{s,max} \tag{5.1}$$

where P_s is the power output. For renewable plants, the lower limit is assumed equal to zero, the upper one is the installed capacity $P_{r,max}$, but the actual production is restricted by the power potentially available, $P_{r,av}$.

For this reason, Eq.(5.1) can be redrafted as follows, distinguishing between conventional and renewable plants:

$$\forall p \in P \quad P_{p,min} \leq P_p \leq P_{p,max} \tag{5.2a}$$

$$\forall r \in R \quad 0 \leq P_r \leq P_{r,av} \leq P_{r,max} \tag{5.2b}$$

Moreover, a cost coefficient c_p or c_r (€/MWh) is assigned to each plant according to its technology (See Sec.7.2).

5.1.2 Loads

The power l_t requested by the sink node t can be valued through its assumed load in percentage $l_{t,\%}$ (see Tab.7.1) and the global system demand L as follows:

$$l_t = l_{t,\%} \cdot L \tag{5.3}$$

5.1.3 Storage systems

In this work, energy storage systems are modelled as devices that can charge and discharge energy given:

- an upper limit of the state of charge $SoC_{b,max}$ expressed in term of (MWh), that is the energy capacity;
- a lower limit of the state of charge $SoC_{b,min}$ in (MWh), that is:

$$SoC_{b,min} = (100\% - DoD_b) \cdot SoC_{b,max} = p_{\%} \cdot SoC_{b,max} \tag{5.4}$$

  where DoD_b is the depth of discharge;
- an upper limit of the rate of charge and discharge $ch_{b,max}$ in (MW), that is the power capacity;
- a charge and discharge efficiency, η_{ch} and η_{dis} respectively; and
- an AC-AC round trip efficiency, $\eta_{ac/ac} = \eta_{ch} \cdot \eta_{dis}$.

The upper limit of the state of charge of the battery $SoC_{b,max}$ is related to $ch_{b,max}$ by the discharge duration, a constant K expressed in hours, and the lower limit $SoC_{b,min}$ is a percentage $p_{\%}$ of the former:

$$SoC_{b,max} = ch_{b,max} \cdot K \tag{5.5}$$
$$SoC_{b,min} = p_{\%} \cdot ch_{b,max} \cdot K \tag{5.6}$$

At the end of each time period j, the state of charge of the storage b, $SoC_{b,j}$, is a function of its initial state $SoC_{b,in}$ and of the incoming or outgoing flow during the period Δj, $ch_{b,j}$ and $dis_{b,j}$ respectively.

$$SoC_{b,j} = SoC_{b,in} + ch_{b,j} \cdot \Delta j - dis_{b,j} \cdot \Delta j \tag{5.7}$$

Moreover, the state of charge has to be included between the upper and lower limits:

$$SoC_{b,min} \leq SoC_{b,j} \leq SoC_{b,max} \tag{5.8}$$

5.2 DC Power flow on a graph

In this section, the DC power flow model explained in Sec.4.1 is brought into the graph structure.

5.2.1 Lines

Each edge $(u, v) \in E$ is defined with a maximum power capacity $c(u, v)$ that can't be exceeded by the flow, which is dependent on the edge's weight $w(u, v)$, set equal to the line's reactance, and the node voltages.

The following equation expresses the above:

$$-c(u,v) \leq \frac{\theta(u) - \theta(v)}{w(u,v)} \leq c(u,v) \tag{5.9}$$

For the sake of convenience, the flow above a generic edge (u, v) is defined as follows:

$$f(u,v) = \frac{\theta(u) - \theta(v)}{w(u,v)} \tag{5.10}$$

Moreover, a "slack bus" must be chosen, as explain in Sec.4.1.

5.2.2 Generators and loads

According to the previous explanation, the power output of a generator $s \in S$ and the power demand of a load bus $t \in T$ are respectively:

$$P_s = \sum_{v \in \Gamma(s)} f(s,v) \tag{5.11}$$

$$l_t = \sum_{v \in \Gamma(t)} f(v,t) \tag{5.12}$$

5.2.3 Storages

Each storage system $b \in B$ is linked to an inner node n by an edge (b, n) with a capacity $c(b, n)$ (MW). Assuming the efficiencies $\eta_{ch} < 100\%$ and $\eta_{dis} < 100\%$, the total inflow and outflow of power in a time step j are calculated as follows:

$$ch_{b,j} = f(b,n)_j \cdot \eta_{ch} \tag{5.13}$$

$$dis_{b,j} = \frac{f(b,n)_j}{\eta_{dis}} \tag{5.14}$$

where $f(b, n)_j$ is the flow through the edge (b, n). In other words, $ch_{b,j}$ and $dis_{b,j}$ are the "internal" flows seen by the storage itself, while $f(b, n)_j$ is the one seen by the external grid.

Since the edge is defined from the storage to the inner node, the flow $f(b, n)_j$ is positive during the discharge and negative during the charge. For this reason, the two cases must be distinguished.

During the discharge, according to Eq.(5.14), Eq.(5.7) is redrafted as follows:

$$SoC_{b,j} = SoC_{b,in} - dis_{b,j} \cdot \Delta j = SoC_{b,in} - \frac{f(b,n)_j}{\eta_{dis}} \cdot \Delta j \tag{5.15}$$

with the constraint in Eq.(5.8) and the following one:

$$\frac{f(b,n)_j}{\eta_{dis}} \leq min\left(\{ch_{b,max}\}, \left\{\frac{SoC_{b,in} - SoC_{b,min}}{\Delta j}\right\}\right) \tag{5.16}$$

This last constraint restricts the outgoing flow to both the maximum rate of discharge of the battery, by an instantaneous point of view, and the amount of energy stored at the beginning of the period.

During the charge, $f(b,n)_j$ is negative, thus, according to Eq.(5.13), Eq.(5.7) is rewritten as follows:

$$SoC_{b,j} = SoC_{b,in} - ch_{b,j} \cdot \Delta j = SoC_{b,in} - f(b,n)_j \cdot \eta_{ch} \cdot \Delta j \tag{5.17}$$

with Eq.(5.8) and:

$$|f(b,n)_j|\eta_{ch} \leq min\left(\{ch_{b,max}\}, \left\{\frac{SoC_{b,max} - SoC_{b,in}}{\Delta j}\right\}\right) \tag{5.18}$$

Eq.(5.18) means that the energy flowing into the battery during the time period Δj cannot be greater than the remaining storage energy capacity, while the instantaneous power flow is limited by the rate of discharge, as said above.

According to Eq.(5.16) and Eq.(5.18), the edge connecting the storage device b and the inner node n has two different capacity limits depending on the direction of the flow:

$$c(b,n) = \begin{cases} ch_{b,max} \cdot \eta_{dis} & \text{when the power flows from } b \text{ to } n \quad (5.19a) \\ \dfrac{ch_{b,max}}{\eta_{ch}} & \text{when the power flows from } n \text{ to } b \quad (5.19b) \end{cases}$$

The constraint about the state of charge can be redrafted as follows:

$$p_{\%} \cdot ch_{b,max} \cdot K \leq SoC_{b,j} \leq ch_{b,max} \cdot K \tag{5.20}$$

5.2.4 Busbars

The busbars are hubs for flows, where the power injected into the grid by generators or storages in discharge phase is directed to loads or storages that are charging. Therefore, the net flow to an inner node n is zero:

$$\sum_{u \in \Gamma(n)} f(u,n) = \sum_{v \in \Gamma(n)} f(n,v) \tag{5.21}$$

5.2.5 Balance between supply and demand

All the power is put into the high voltage lines and transmitted to consumers, maintaining a continuous balance between electricity supply and demand.

Given a time period j, Eq.(5.22) brings together all the actors of the model:

$$\sum_{p \in P} P_{p,j} + \sum_{r \in R} P_{r,j} + \sum_{b \in B} f(b,n)_j = \sum_{t \in T} l_{t,j} \tag{5.22}$$

5.3 Minimization of daily production costs

The aim of this work is the minimization of production costs over a determined time horizon, reducing the renewable power curtailment by means of electrochemical storage systems.

5.3.1 Time series: 24-hours horizon

The application of demand and generation time series to power flow can be advantageous with high levels of variable renewable generation in transmission systems. Half hourly or quarterly time steps can be used to consider the load variations and the volatility of RES over a day.

In this work, we take into account a 24-hours horizon and a quarterly resolution. For this reason, all flows are to be considered as average values of a quarter-hour j, with j from 0 to 95.

Moreover, the state of the grid at the end of a time step j represents the initial state of the next one $j + 1$.

5.3.2 Renewable power curtailment

When the available renewable production is too high to fulfil the constraint of balance or transmission capacity, then only a limited part of this is injected into the grid, while the one in excess is cut off.

The amount of curtailed RES energy (MWh) in the 24-hours horizon, with a quarterly resolution, can be valued as follows:

$$curtailment = 0.25 \sum_{j=0}^{95} \sum_{r \in R} (P_{r,j,av} - P_{r,j}) \tag{5.23}$$

With the aim of minimizing the curtailment of wind or solar production, this solution is penalized with a high cost $curt\_cost$.

5.3.3 Objective function

The daily system cost to be minimised is defined as follows:

$$min \sum_{j=0}^{95} \left[\sum_{p \in P} c_p \cdot P_{p,j} + \sum_{r \in R} c_r \cdot P_{r,j} + curt\_cost \cdot \sum_{r \in R} (P_{r,j,av} - P_{r,j}) \right] \tag{5.24}$$

where c_p and c_r are the cost coefficients in Tab.7.3.

The following linear constraints must be fulfilled:

- Upper and lower power generation limits $\forall p \in P$

$$P_{p,min} \leq P_{p,j} \leq P_{p,max}$$

- Upper and lower power generation limits for RES plants $\forall r \in R$

$$0 \leq P_{r,j} \leq P_{r,j,av} \leq P_{r,max}$$

- Transmission line capacity $\forall (u,v) \in E$

$$-c(u,v) \leq f(u,v)_j \leq c(u,v)$$

- Fulfilment of power demand $\forall t \in T$

$$\sum_{v \in \Gamma(t)} f(v,t)_j = l_{t,j}$$

- Flow conservation $\forall n \in N$

$$\sum_{(u,n) \in E} f(u,n)_j = \sum_{(n,z) \in E} f(n,z)_j$$

- Balance between supply and demand

$$\sum_{p \in P} P_{p,j} + \sum_{r \in R} P_{r,j} + \sum_{b \in B} f(b,n)_j = \sum_{t \in T} l_{t,j}$$

- Power and energy flows $\forall b \in B$ if $f(b,n) > 0$

$$\frac{f(b,n)_j}{\eta_{dis}} \leq min \left(\{ch_{b,max}\}, \left\{ \frac{SoC_{b,j-1} - SoC_{b,min}}{\Delta j} \right\} \right)$$

- Power and energy flows $\forall b \in B$ if $f(b,n) < 0$

$$|f(b,n)_j|\eta_{ch} \leq min\left(\{ch_{b,max}\}, \left\{\frac{SoC_{b,max} - SoC_{b,j-1}}{\Delta j}\right\}\right)$$

- State of charge $\forall b \in B$

$$p_{\%} \cdot ch_{b,max} \cdot K \leq SoC_{b,j} \leq ch_{b,max} \cdot K \tag{5.25}$$

  where $SoC_{b,j}$ is defined in Eq.(5.15) during the discharge and in Eq.(5.17) during the charge.

- Phase angle constraints:

$$\begin{aligned} &\frac{-\pi}{2} \leq \theta_{v,j} \leq \frac{\pi}{2} \quad \forall v \in V \setminus s : \text{slack bus} \\ &\theta_{s,j} = 0 \quad s : \text{slack bus} \end{aligned}$$

6

Optimization tool

[1] A software was developed in order to minimise the objective function Eq.(5.24), starting from an input file with the grid description and renewable production profiles.

6.1 Software Structure

The software is composed by three main sections, all managed by a Controller.

6.1.1 Instance Manager

The first section is called "*Instance Manager*". It elaborates and manages the data and is composed by three classes:

- *Data elaborator*. It manages all data transformations during the simulation in two main ways. On the one hand, it elaborates the input file with row data of the grid as a graph and of the renewable profiles and creates an instance with a graph for each time period; on the other hand, it uses the data of the storage in the graph of the instance j to update the same ones of the instance $j + 1$, according to Eq.5.7.
- *Parser*. This class processes and parses both the input row data and those that describe the grid status after the optimization of j-th instance, which are also updated.
- *Instance printer*. It manages the program output, by arranging the instance data for the solver and by formatting the storage final data.

[1] For more details about the developed software, refer to [41]

6.1.2 Data abstraction

This section provides the data structures required to manage the power system information and is composed by three main classes, containing sub-classes:

- *Node*. It classifies nodes into three sub-classes, i.e. consumer, generator, storage, according to the main characteristics of the components described in Sec.5.1 and summarised in Tab.6.1.

Table 6.1: Properties of the three sub-classes of class "Node"

Sub-Class	**Properties**	**Description**
Consumer	Load	asssumed load in percentage $l_{t,\%}$
Generator	Max prod	upper limit $P_{s,max}$
	Min prod	lower limit $P_{s,min}$
	CostCoeff	cost coefficient c_s
	Type	Thermal or Renewable
Storage	MinCapacity	lower limit of SoC $SoC_{b,min}$
	MaxCapacity	upper limit of SoC $SoC_{b,max}$
	Availability	available energy SoC SoC_b

- *Edge*. It describes the properties of each edge of the graph, that is "Weight", "Capacity" and "Flow".
- *Graph*. It uses the above classes to represent the graph structure, that is described by a matrix $n \times n$, where n is the total number of node. If the capacity of an edge (u, v) is equal to zero, then u and v are not linked. Moreover, there is a list containing all grid vertexes.

6.1.3 Model objects

This module contains the three main elements required for the optimization:

- *Instance data*. The instances created by Data elaborator are ready to be optimised.
- *Core model*. It is the mathematical formulation of the problem in MathProg language.
- *Solver*. It optimises the instances according to the mathematical formulation in Core model.

6.1.4 Controller

The Controller is the main routine that manages the different activities of the software during its execution. The main steps are the following:

1. Managing of the input.
2. Parsing of grid data and creation of instances.
3. Resolution routine: a phase of creation and resolution of an instance alternates with the grid data updating for the next one.
4. Printing of final data and information about the process.

6.2 Implementation

6.2.1 Linear programming problem

According to the DC power flow model seen in Sec.4.1, the problem is expressed as a *linear programming problem*.

The linear programming is a mathematical method of solving practical problem (e.g. allocation of resources, maximization of profit or minimization of costs) by means of linear functions, where the variables involved are subjected to constrains. In this work, the optimal solution is found with the simplex method which guarantees the results optimality if the problem converges.

6.2.2 GLPK Library for optimization

The GLPK (GNU Linear Programming Kit) is a software package intended for solving large-scale linear programming (LP), mixed integer programming (MIP), and other related problems. It is a set of routine written in ANSI C and organized in the form of a callable library [19]. The GLPK package includes the components listed below [19]:

- primal and dual simplex methods;
- primal-dual interior-point method;
- branch-and-cut method;
- translator for GNU MathProg;
- application program interface (API); and
- stand-alone LP/MIP solver *glpsol*.

6.2.3 Languages

The software is written by means of two languages:

- Java SE 7 (1.7.0). The majority of the program is written Java, in particular the sections Instance Manager, Controller and Data abstraction.
- GNU MathProg. This language is used mainly in the section Model objects for the mathematical formulation of the problem and the instances creation.

MathProg

The main problem and the instances are modelled in *GNU MathProg Modeling Language*, whose syntax is partially shared with *AMPL* language. A MathProg program has extension .mod and it is usually structured in five sections:

- *"Variable Definitions"* where all the parameters and variables are declared;
- *"Objective Function"* namely the function that has to be minimised or maximised;
- *"Contraints"* to which the variables are subjected;
- *"Data"* where the parameters' values are defined. Sometimes this section is reported in an external file; and
- (Optional) *"Results"* where the solution is displayed.

7

Test case: HV system with renewable generation and storage devices

7.1 The IEEE Reliability Test System-1996

In this work, a modified version of the IEEE Reliability Test System 1996 (RTS-96) is used as case study [43]. This test system is developed by modifying and updating the original IEEE RTS published in 1979 (RTS-79) [34]. The topology of RTS-79 is shown in Fig.7.1 and is labelled "Area 1".

In 1996, the task force decided to develop a multi-area reliability test system by linking various RTS-79 areas. Fig.7.2 shows a three-area system developed by merging three single areas ("Area 1", "Area 2" and "Area 3") through five interconnections:

- 51-mile 230-kV line connecting bus #123 and bus #217
- 52-mile 230-kV line connecting bus #113 and bus #215
- 42-mile 138-kV line connecting bus #107 and bus #203
- 72-mile 230-kV line connecting bus #223 and bus #318
- 67-mile 230-kV line connecting bus #121 and bus #325

A phase shift transformer has been added between bus #325 and #323 in "Area 3". An optional DC link connects "Area 1" at bus #113 to "Area 3" at bus #316.

The buses for "Area 1" are labelled with numbers ranging from 101 through 124; for "Area 2" from 201 to 224 and for "Area 3" from 301 to 325. There are:

- 96 generators (18 hydro and 78 thermal)

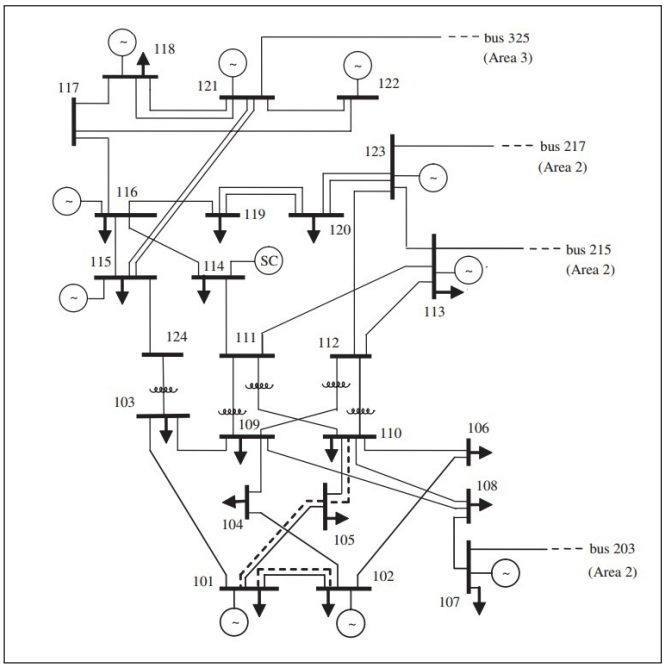

Figure 7.1: IEEE RTS-96 Area 1

- 73 nodes
- 120 edges (lines and transformers)

The total installed production capacity amounts to 10215 MW, while the assumed peak load is 8550MW. Table 7.1 shows the assumed load for each bus of the three areas.

Table 7.2 shows the generator data that are taken into account in this paper. It has to be noted that the lowest power for each kind of technologies is an added parameter and valued by considering technical limits of different components, e.g. boiler and prime mover.

All *per unit* (pu) quantities are on 100MVA base power.

7.2 Technologies and costs

The first aim of a vertical integrated power system is the fulfilment of customers' demand, maintaining high quality service. The generation technologies that are mostly used today are:

- *Intermittent/Non dispatchable renewable energy*: PV solar and wind;
- *Baseload generation* ($\geq 4000h/y$): nuclear, coal-fired steam power plants, run-of-the-river hydro and partly-adjustable conventional hydro, geothermal, biomass-fired steam plants;

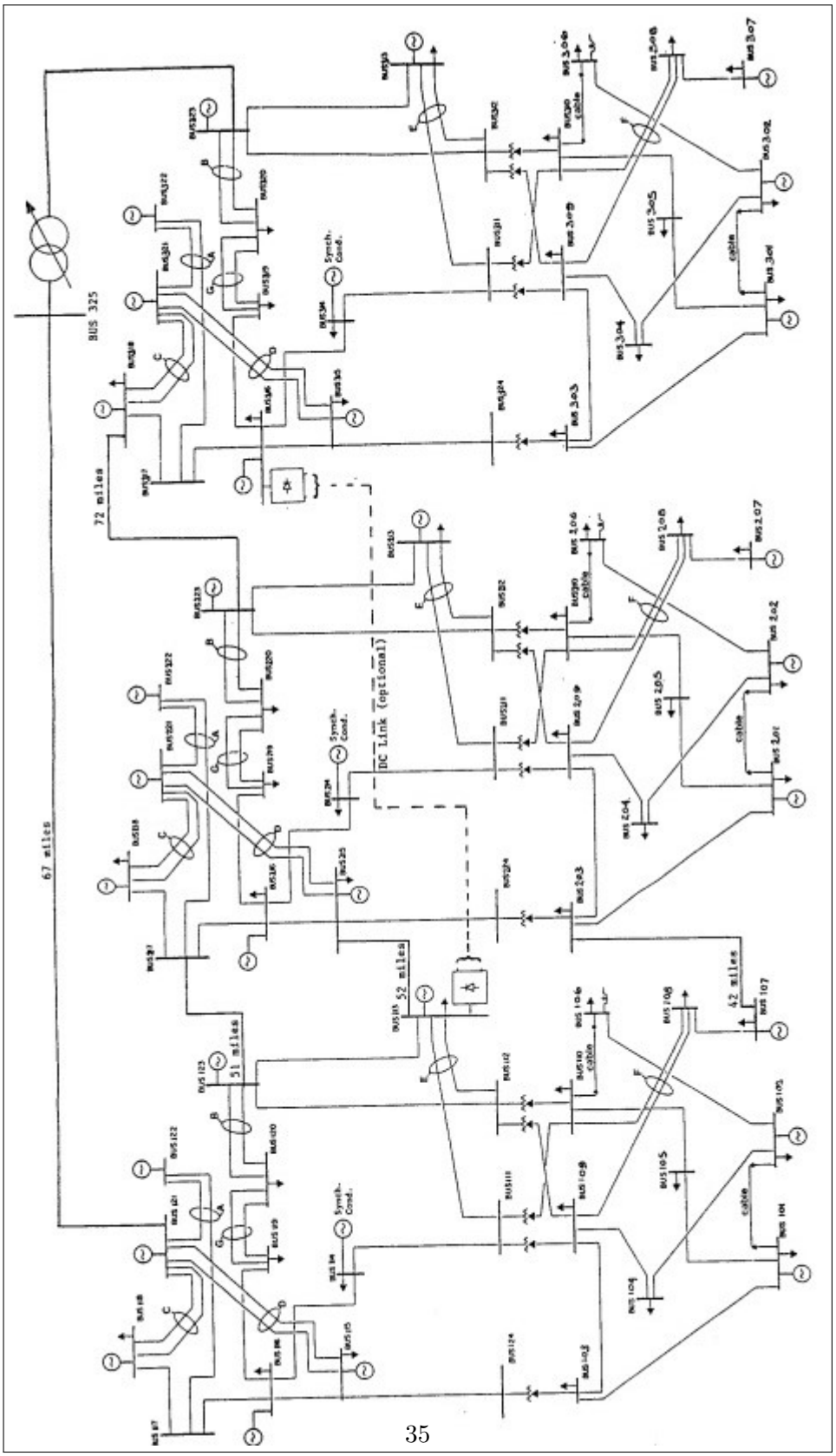

Figure 7.2: IEEE RTS-96 Three areas

Table 7.1: Bus load data

Bus number	**Bus load**
	% of system load
101,201,301	3.8
102,202,302	3.4
103,203,303	6.3
104,204,304	2.6
105,205,305	2.5
106,206,306	4.8
107,207,307	4.4
108,208,308	6.0
109,209,309	6.1
110,210,310	6.8
113,213,313	9.3
114,214,314	6.8
115,215,315	11.1
116,216,316	3.5
118,218,318	11.7
119,219,319	6.4
120,220,320	4.5
Total	100.0

Table 7.2: Generator data

Unit group	**Unit size**	**Unit Type**	**Lowest output**
	MW		%
U12	12	Oil/Steam	40
U20	20	Oil/CT	40
U50	50	Hydro	0
U76	76	Coal/Steam	50
U100	100	Oil/Steam	40
U155	155	Coal/Steam	50
U197	197	Oil/Steam	40
U350	350	Coal/Steam	50
U400	400	Nuclear	75

- *Intermediate generation* ($1000-4000h/y$): combined cycle gas turbines (CCGT), fully-adjustable conventional hydro;
- *Peaking and stand by generation* ($\leq 1000h/y$): open cycle gas turbine (OCGT), oil-fired steam power plants, pumped-storage hydro and peak conventional hydro.

For each technology, fixed and variable costs have to be taken into account. The fixed costs are expressed in terms of (k€/MW per year) and consist of investment cost and fixed operation and maintenance cost. The variable ones consist in fuel and variable O&M cost, both expressed in terms of (€/MWh). All these costs are very much related to plant's size.

The concept of *marginal cost* has to be introduced. The *marginal cost* is the change in the total cost that arises when the quantity produced is incremented by one unit, that is, the cost of producing one more unit of a good [35]. In power systems, the marginal cost allows to compare the added cost of increasing production by one unit from different sources and it includes operating costs and fuel costs.

In this paper, six technologies are included: oil, coal, nuclear, conventional hydro (fully-adjustable and peak), wind and solar. In order to determine the optimal mix, we consider a *cost coefficient* expressed in terms of (€/MWh) for each technology, according to the size of the power plant (Tab. 7.3).

About hydro units, we consider a very small cost coefficient during peak load hours, while during the off-peak hours these plants are not committed to produce. Their marginal cost, in fact, is low, but it is a high-value energy, since available in any eventuality. For this reason, hydroelectric plants with big seasonal capacity as well as pumped-storage ones are usually used as peaking power plants. In this work, these plants are considered available only when the quarterly load demand is higher then 70% of the daily maximum peak.

Table 7.3: Cost coefficients

Unit type	**Unit size**	**Cost coefficient**
	MW	€/MWh
Oil/Steam	12	80
Oil/CT	20	70
Oil/Steam	100	60
Oil/Steam	197	55
Coal/Steam	76	55
Coal/Steam	155	45
Coal/Steam	350	40
Nuclear	400	35
Hydro	50	10
Wind	0.02	0.5
Solar	0.2	1.25

7.3 Renewable Energy Sources

7.3.1 Addition of renewable plants

We use the RTS-96 grid as the starting point for our evaluation. In particular, we first add renewable plants for a total capacity equal to 0%, 10%, 20%, 30%, 40%, 50%, 66% and 74% of winter global load demands. The new suppliers are placed by considering the following policies:

- cutting the 3, 6, 12 or 15 longer transmission lines, that is 1, 2, 4 or 5 per area, and adding a new internal node, a wind generation node and a dummy edge;
- adding also a new solar-PV generation node and a dummy edge to 9 or 12 load buses, that is 3 or 4 per area.

The different scenarios are summarized in Tab.7.4.

Table 7.4: Additional generation

	Wind farms	**Solar-PV farms**	**Total**
10% PV + W	3 x 200 MW	9 x 44 MW	996 MW
20% PV + W	6 x 200 MW	12 X 64,5 MW	1974 MW
30% PV + W	15 x 170 MW	9 X 48 MW	2982 MW
40% PV + W	15 x 220 MW	12 X 55 MW	3960 MW
50% PV + W	15 x 285 MW	12 x 55 MW	4935 MW
66% PV + W	15 x 350 MW	12 X 55 MW	5910 MW
74% PV + W	15 X 400 MW	12 x 55 MW	6660 MW

7.3.2 Renewable production profiles

Renewable power injections are estimated using deterministic production profiles extracted from historical wind and solar-PV generation data of two farms located in central Italy.

Solar-PV generation

Fig.7.3 shows the historical hourly power generated from a 200-kW solar-PV plant during one year.

A typical daily solar-PV generation profile is displayed in pu in Fig.7.4a. Once chosen four random days, one per season, one can see that the peak production is always around noon, while the value varies from 18% to 90% of installed capacity.

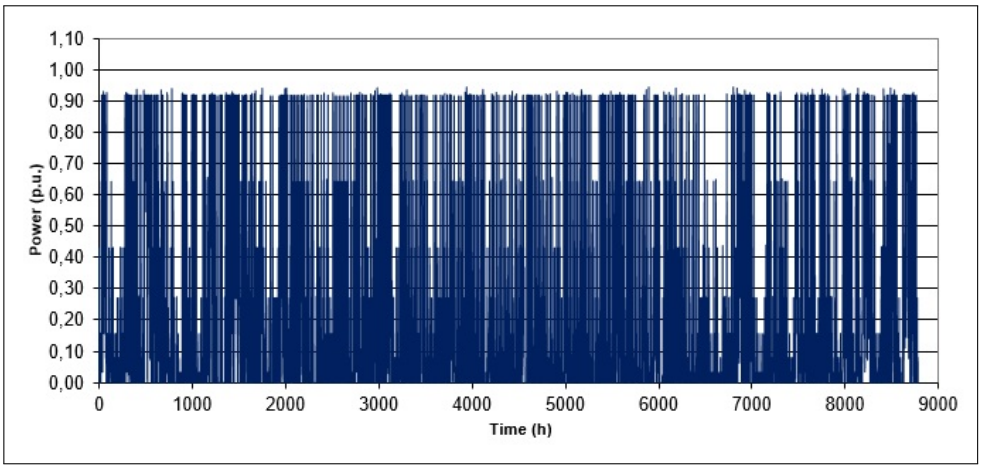

Figure 7.3: Example of historical hourly power output of a 200-kW solar-PV plant

Wind generation

The wind generation is more varying than the solar one and the peaks can appear equally during the daytime or during the night. Given a yearly wind speed profile as the one shown in Fig.7.5, the production of a wind turbine Vestas V90-2.0 MW could be the one in Fig.7.6. The V90's data are reported in Tab.7.5.

Table 7.5: Wind turbine data

P nom	2 MW
Efficiency	0.92
V cut on	4 m/s
V nom	12 m/s
V cut off	25 m/s

As done for the solar generation, we consider four days of wind production, whose trend is showed in Fig.7.4b.

Using the above data, 96 values for each day are extrapolated to simulate the variable renewable production.

7.4 Load demand

All load data are taken from [38], where the national load demand of the third Wednesday of each month of 2012 are recorded. We consider four months (January, April, July and October) to analyse different production-demand situations.

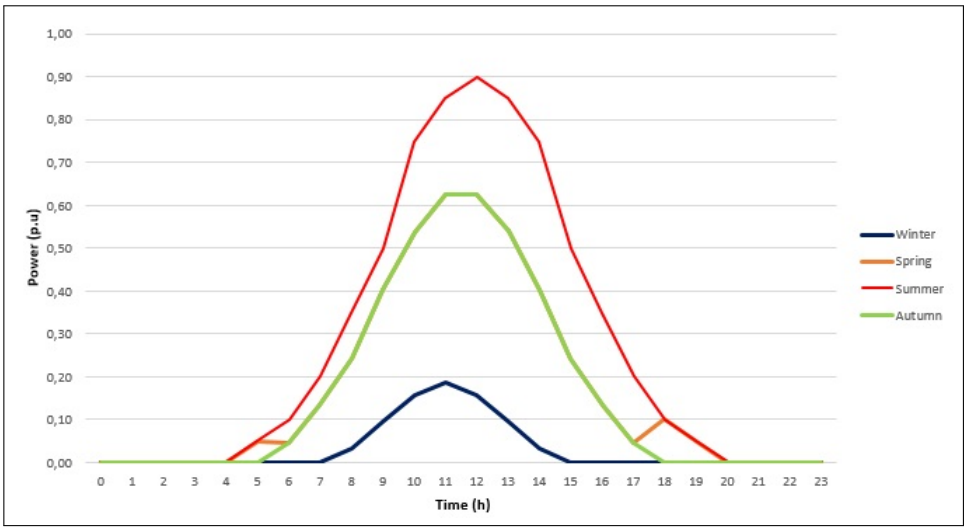

(a) Solar-PV

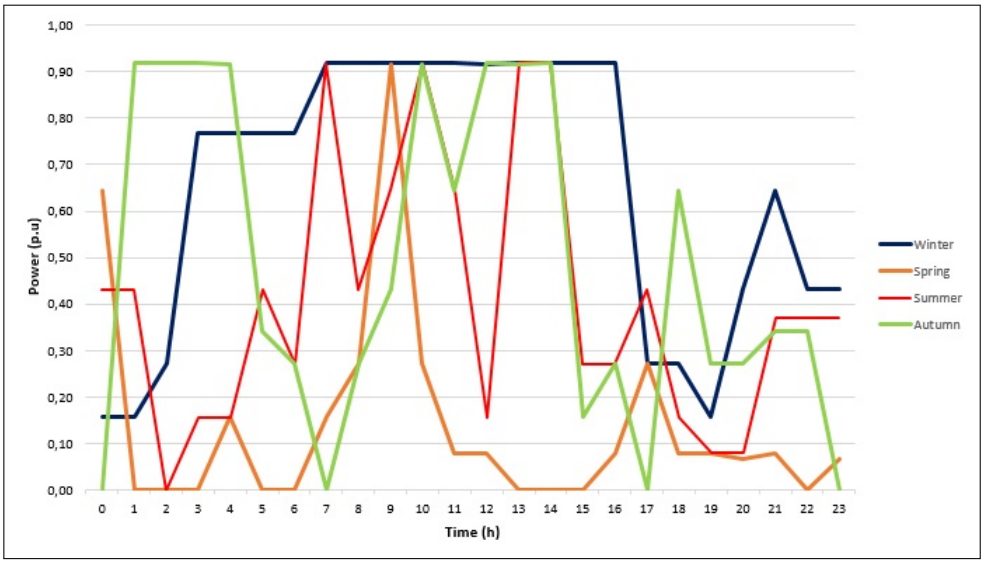

(b) Wind

Figure 7.4: Daily renewable generation profiles

Since the total installed production capacity in the RTS-96 amounts to 10215 MW, which is considerably lower than the Italian value, all data have to be adjusted. In Tab.7.6 the maximum daily values are reported.

In 2010, the available average power during the winter peak, which is defined as the "average power that was supplied by generation plants to meet the daily peaks of the winter period" [37], was estimated at around 69.3 GW, the 65% of the installed capacity (106.5 GW). In 2012, this latter was 123.5 GW, thus the available average power can be evaluated at 80.3

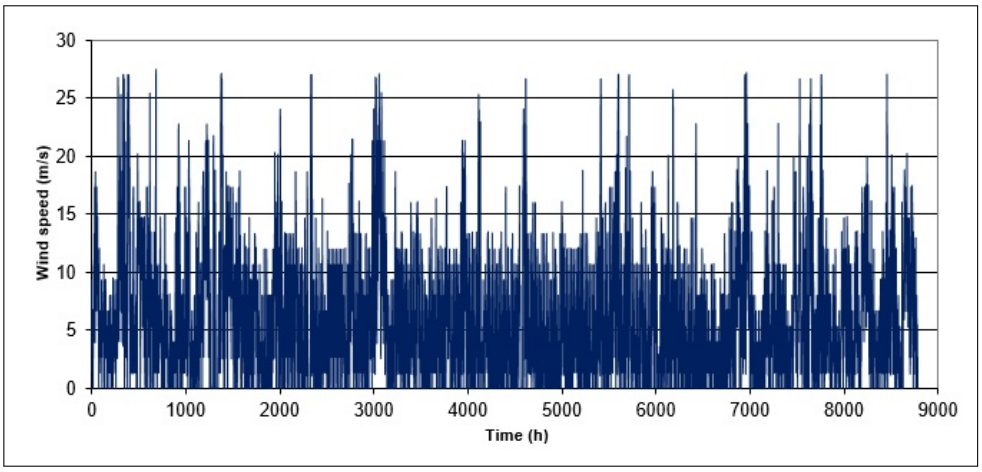

Figure 7.5: Yearly wind speed profile

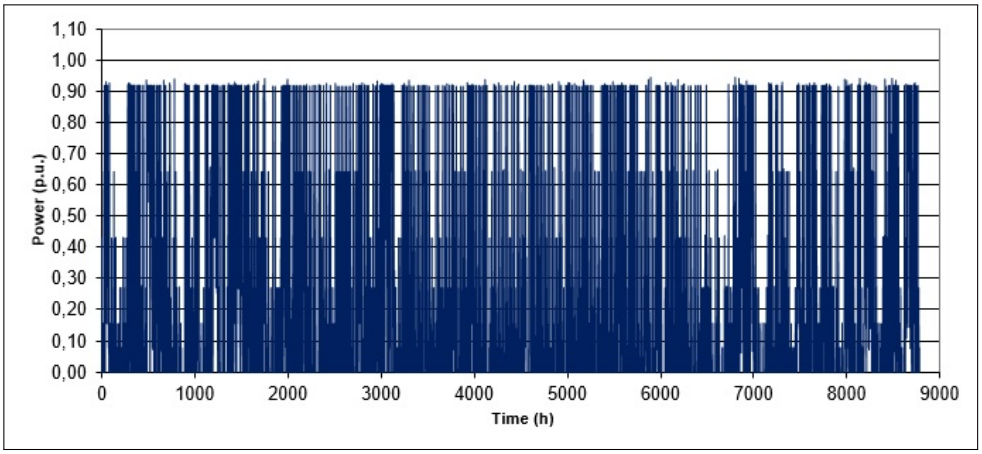

Figure 7.6: Average hourly power output of a V90-2 MW in p.u.

GW. Since the annual peak load was 54.1 GW, their share was 67.4%.

In our work, all the plants are running, thus the available power corresponds to the installed one. Adding an amount of renewable power equal to the 45% of the peak load, according to [38], the winter maximum demand is set to 9866 MW. The other seasonal peaks are adjusted by reducing the national load demand to its 19%.

Fig.7.7 shows the four load curves, with typical seasonal Italian trends.

Table 7.6: Seasonal maximum load demand

Season	**Maximum demand**
	MW
Winter	9866
Spring	8652
Summer	9716
Autumn	8559

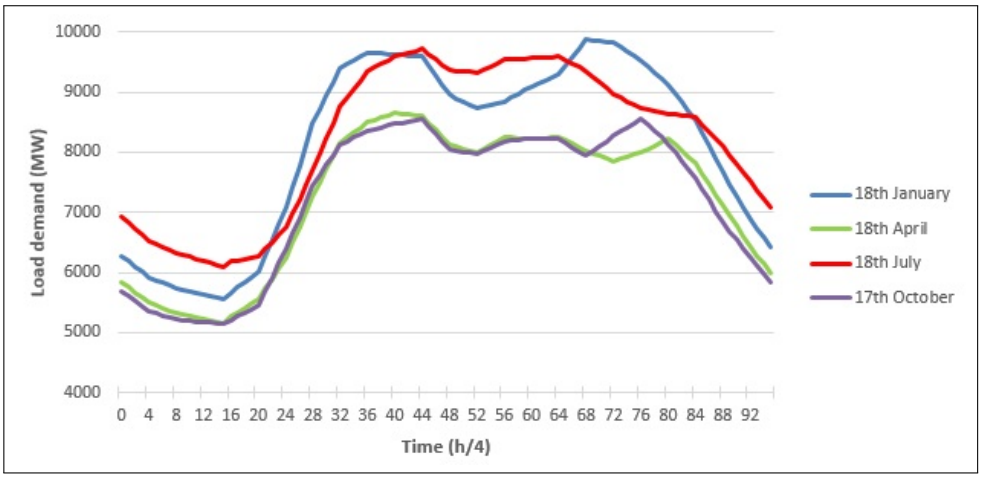

Figure 7.7: Load curves

7.5 Topological representation of the updated RTS-96

A representation of the updated version of IEEE RTS-96 as a graph is shown in Fig.7.8. One can refer to that graph for scenarios with 15 wind farms, 12 PV-solar plants and storages located near the former ones.

The capacities of "real" edges are reduced to their 75%, since we are not interested in having a system operated in an "N-1" security state, that is if any single component outages does not lead to a cascading failure, but rather in understanding the network behaviour under critical condition.

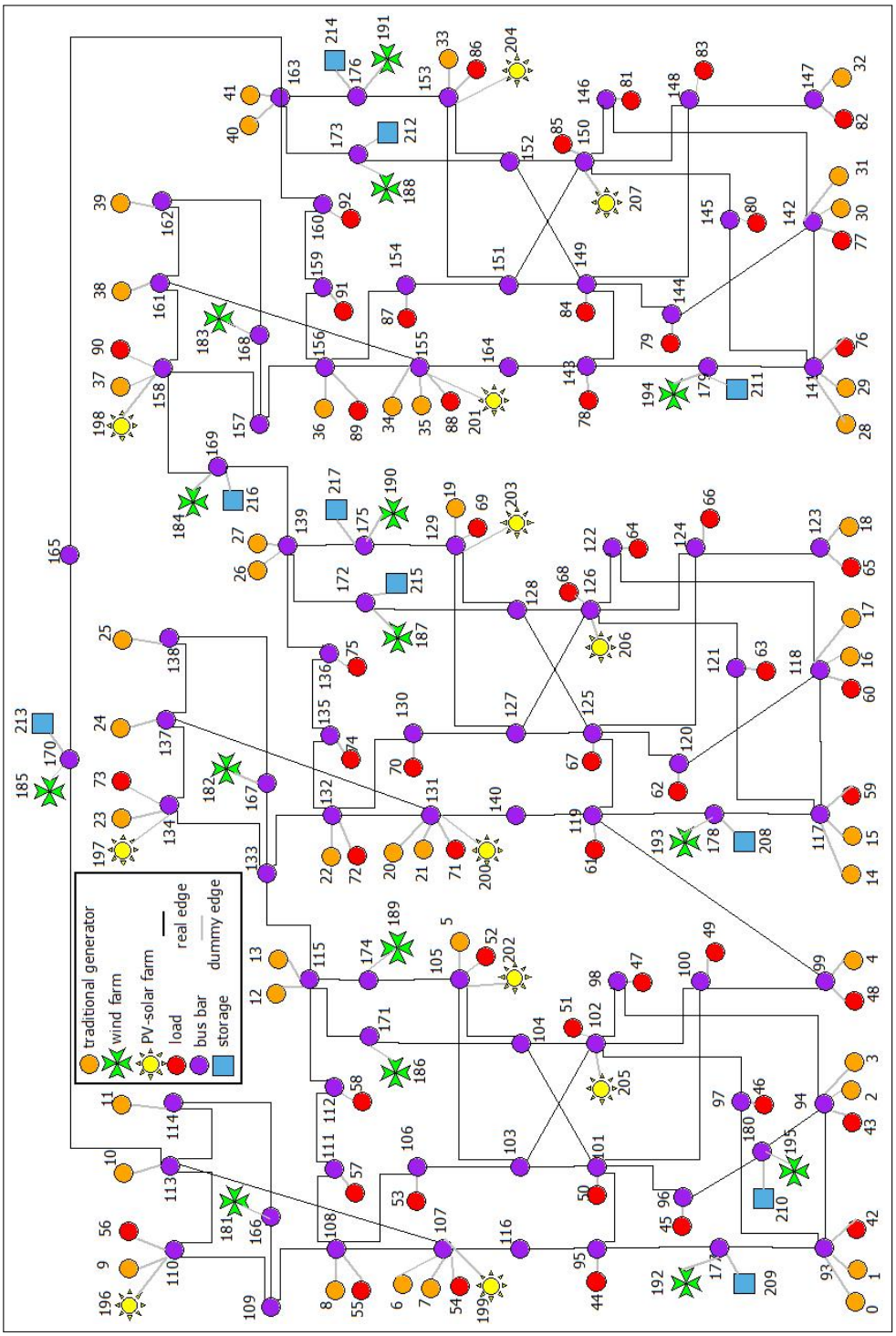

Figure 7.8: A version of the updated IEEE RTS-96 as a graph

8

Simulation

8.1 Setup

8.1.1 Hardware and software

For this work, a laptop with the following specifications is used:

- OS: Ubuntu 14.04 LTS 64bit;
- processor: Inter®Core^{TM}i5-2430M CPU 2.40 GHz * 4; and
- RAM: 8 Gb DDR3.

The software developed to run all simulations is written in Java SE 7 (1.7.0) and GNU MathProg (Sec.6.2.3), and it is made to be used is Linux-based systems.

8.1.2 Data

The test case is developed by modifying the IEEE RTS-96. All data of the last one can be found in [43], while the changes are described in Sec.7.3 and Sec.5.2.3.

8.1.3 Metrics

The aim of this work is understanding the network behaviour under critical condition. To identify the lines that tend to be overloaded and the ones that carry the greatest portions of power, we propose two metrics and we value the benefits of the use of storages through the estimate of the curtailed energy. Moreover, the exploitation of these devices is valued both in terms of time and performance.

Lines

- The *Centrality Index* $\widehat{C_f}(e)_j = \sum_{u \in S} \sum_{v \in T} \frac{f_{e,j}}{f_{max,j}} \cdot 100$ indicates those edges over which the greatest portions of power flow during the period j, where $f_{max,j}$ is the maximum flow from the node u to the node v and $f_{e,j}$ the rate passing through the edge e. By considering the whole set of sources S and sinks T, $f_{max,j}$ is equal to the total power flowing above the grid in j, that is equal to the global load demand in the same time period, and $f_{e,j}$ is the flow on the edge e.

  First of all, the daily average index is valued for each edge, then, since this parameter depends on the total load demand in j, we calculate the daily average load demand as $\frac{\sum_{j=0}^{95} \sum_{t \in T} l_t}{96}$. Lastly, using these four average values as weights, we estimate a weighted mean for each edge.

- The *Utilization Index* $U(e)_j = \frac{f_{e,j}}{c_e} \cdot 100$ expresses how much an edge e is exploited in percentage of its capacity, where $f_{e,j}$ is the power flowing on the edge during the time step j and c_e its capacity.

  If an edge reaches its limit, then the daily number of quarters of hour in which this occurred is counted and the sum over four days is valued.

Curtailment

- Given a renewable plant r, the power injected into the grid $P_{r,j}$ during the time step j is limited not only by the power potentially available $P_{r,av,j}$ according to the weather condition, i.e. the windiness and solar radiation, but also by the capacity of the power system to transport and absorb it. For this reason, the *curtailed renewable power* is valued as $P_{r,av,j} - P_{r,j}$.

- The amount of *curtailed RES energy* in the 24-hours horizon is valued as $curtailment = 0.25 \sum_{j=0}^{95} \sum_{r \in R} (P_{r,j,av} - P_{r,j})$, considering a quarterly resolution.

Storages

- The number of quarters of hours during which a storage b is used is valued by counting the time steps when $SoC_{b,j} > SoC_{b,min}$.

- Given a certain grid scenario, the performance of a storage b is valued by calculating in four days the average of the maximum energy stored and the average of the maximum power injected or extracted.

In this way, given a set of storages, we try to identify their best locations according to their exploitation and, in case, an excess of power/energy capacity.

8.2 Software performance

Some performances measurements are made to estimate the run-time and the use of memory by glpsol solver with the increasing of number of nodes, Fig.8.1

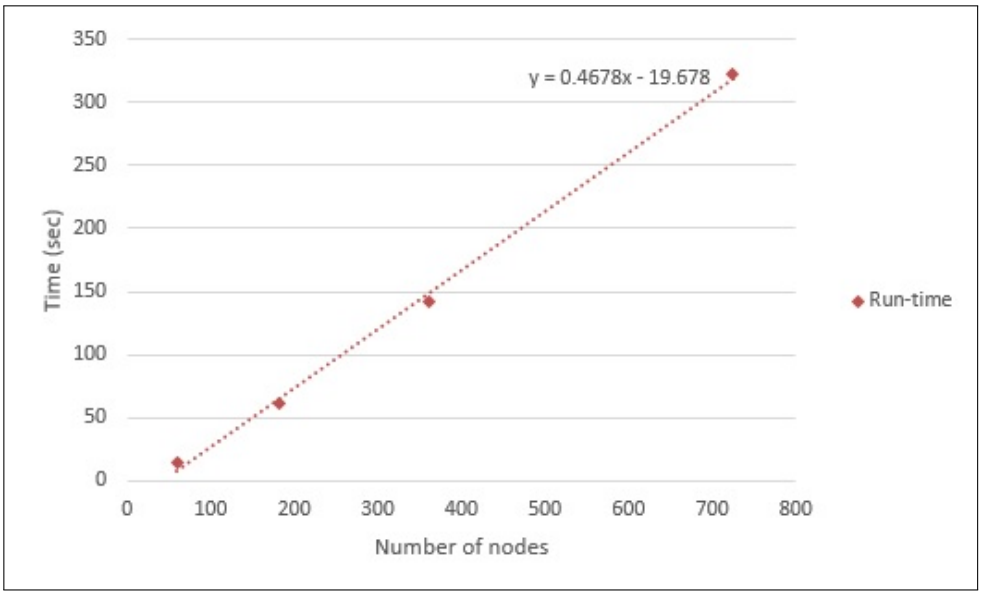

(a) Run-time

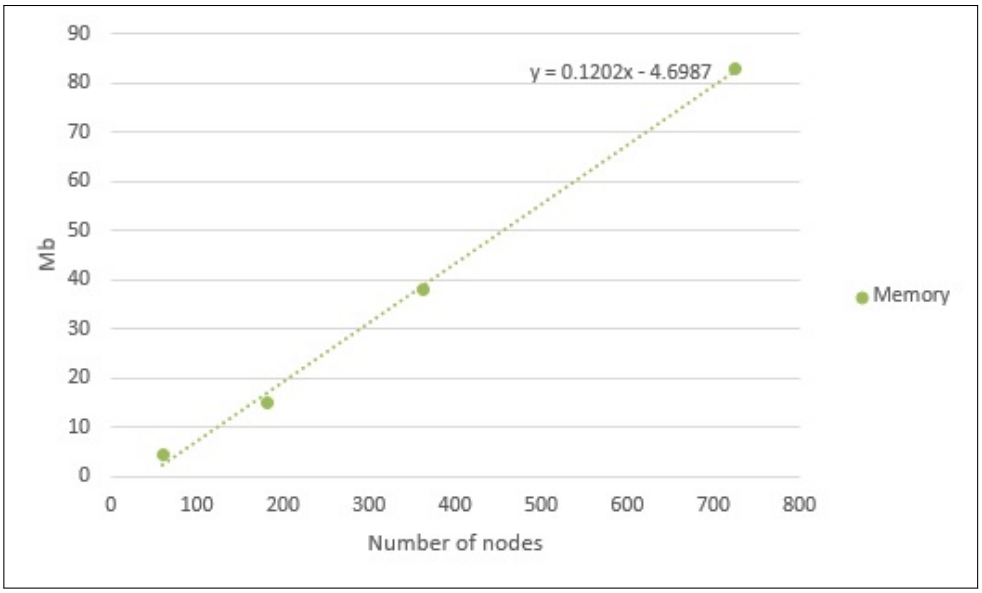

(b) Use of memory

Figure 8.1: Performances

8.3 Run

8.3.1 From input to output

Starting from the data of the modified version of IEEE-RTS 96, a txt input file is written for each scenario and imported in the developed software (Sec.10.1). Around 74 sec are required to elaborate the file, model all the components of the network, find the optimal solution of our objective function minimization and print the output data.

The results of each simulation without storage are included in 96 text files, which provide the power curtailed for each renewable plants and the following informations for each edges, during the time period j:

- the power flow, $f_{e,j}$;
- the utilization index, $U(e)_j$, defined in Eq.(4.22);
- the normalized flow-based centrality index, $\widehat{C_f}(e)_j$, defined in Eq.(4.21).

If some storages are integrated into the grid, then one more text file is generated, reporting the initial level of stored energy in every device and its state of charge at the end of each quarter-hour (Sec.10.2).

8.3.2 Results before storage systems integration

By means of the developed program, we simulate the grid with seven different percentage of renewable installed capacity and in four days of the year, in order to analyse different supply-demand scenarios, as already explain in Sec.7.3 and Sec.7.4.

Wind and solar productions are intermittent and volatile, so that the grid is not always able to totally absorb them due to transmission and operating constrains.

Tab.8.1 reports the curtailed energy for each supply-demand scenario and the sum over 4 days.

Fig.8.2 shows an example of comparison between load demand, renewable and conventional productions, and curtailed energy. The power curtailment is essentially required before 6 a.m., due to high available RES power coinciding with low demand, while the conventional production is maintained at its lower level as long as possible. This one is dispatched according to the marginal cost of each plant, so that nuclear and the cheapest coal plants cover the baseload demand, that is 63% of the total production on average, the hydro ones are called to supply when the load is higher than 70% of the maximum, and the oil ones are kept at their minimum technical output (Fig.8.3). Of course, the greater the installed renewable capacity, the more frequent and higher the necessity of curtailing its output.

Table 8.1: Curtailed energy for every supply-demand scenario

	Winter MWh	**Spring** MWh	**Summer** MWh	**Autumn** MWh	**Total** MWh
10%	0	0	0	550	550
20%	184	0	0	2 755	2 939
30%	2 591	753	0	7 784	11 128
40%	4 422	1 258	81	11 107	16 867
50%	8 250	2 458	1 448	18 208	30 363
66%	17 003	4 135	5 241	26 029	52 408
74%	26 635	5 425	90 001	32 773	15 4834

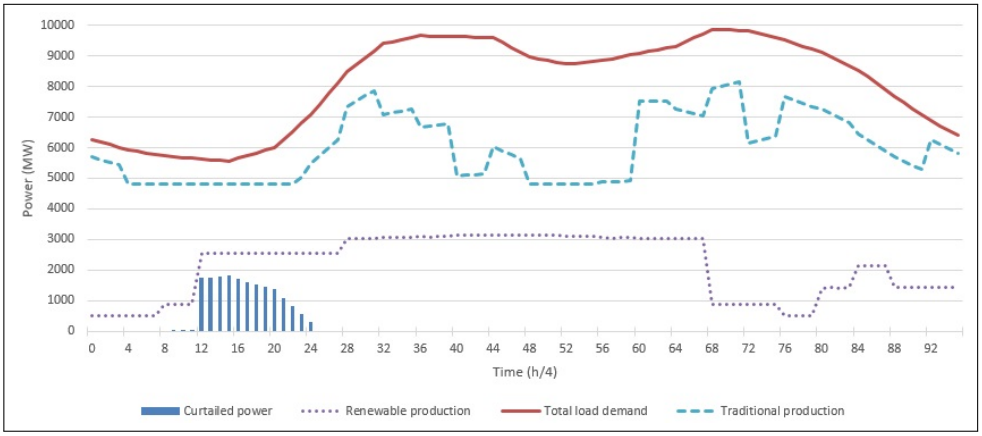

Figure 8.2: Comparison between supply, demand and curtailment in Winter with 40% of RES installed capacity

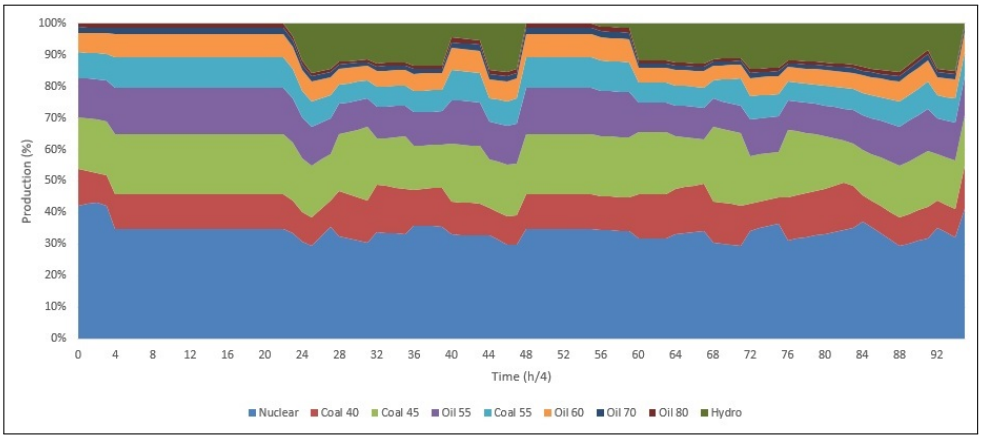

Figure 8.3: Dispatching of conventional plants

Table 8.2: Curtailed energy from Solar-PV farms

Scenario	**Winter**		**Spring**		**Summer**			**Autumn**				**Total**
Node	**66%**	**74%**	**66%**	**74%**	**50%**	**66%**	**74%**	**40%**	**50%**	**66%**	**74%**	**MWh**
196	0	0	0	0	0	0	0	0	0	0	0	0
197	0	0	0	0	0	0	0	0	0	0	0	0
198	0	0	11	6	6	12	49	0	64	101	111	361
199	0	0	0	0	0	0	0	0	0	0	0	0
200	0	0	0	0	0	0	0	0	0	0	0	0
201	2	2	17	21	9	14	34	4	101	117	151	472
202	0	0	0	0	0	0	0	0	0	0	0	0
203	0	3	0	0	0	3	16	0	3	46	40	111
204	4	9	5	11	10	12	12	23	94	110	125	415
205	0	0	0	0	0	0	0	0	0	0	0	0
206	0	6	6	11	3	9	11	0	40	72	90	247
207	9	12	16	20	10	35	69	39	116	133	151	611
Total	15	32	55	69	38	85	191	66	418	579	668	

It is worth to notice that the curtailment affects mainly the wind farms, but also the solar ones from 40% of renewable installed capacity. Tab.8.2 reports the daily and total amount of energy curtailed at each of these ones. Farms 198, 201, 204 and 207 are the most involved.

It's interesting to remark that the PV plants are added on buses with high load demand, so that the power required is usually higher than the power generated by these farms and they do not inject power into the rest of the grid, whereas it is not even enough to fulfil the load.

For this reason, in our analysis lines are divided in "real" and "renewable": the former group includes all the edges, apart from the dummy ones, since they are not real transmission lines, as described in Sec.4.4, while the latter just the ones linked to a wind farm.

Tab.8.3 reports the daily average centrality index for the top 3 real edges and renewable ones in each scenario. The triplet of lines {131-137, 155-161, 107-113} has always the highest values, with a decreasing trend as RES capacity increases. In Fig.8.4 their weighted mean over four days is shown (See Sec.8.1.3).

About the edges linked to wind farms, it should be noted that the grid configuration changes by adding more plants, and it remains the same from 30% scenario onwards. Fig.8.5 shows the trends of the lines {152-173, 128-172}, which are in the top 3 in all cases and they tend to grow up, even if not sharply.

Table 8.3: Centrality index: top 3 daily average values before storage integration

	Winter				Spring				Summer				Autumn			
	Line Real	**$C(e)_{av}$ %**	**Line Ren**	**$C(e)_{av}$ %**	**Line Real**	**$C(e)_{av}$ %**	**Line Ren**	**$C(e)_{av}$ %**	**Line Real**	**$C(e)_{av}$ %**	**Line Ren**	**$C(e)_{av}$ %**	**Line Real**	**$C(e)_{av}$ %**	**Line Ren**	**$C(e)_{av}$ %**
	131-137	4.84	157-168	1.95	131-137	5.28	157-168	1.48	131-137	4.87	157-168	1.71	131-137	5.40	133-167	2.04
10%	155-161	4.41	133-167	1.95	155-161	4.53	133-167	1.47	155-161	4.53	133-167	1.70	155-161	4.67	109-166	1.95
	107-113	4.01	109-166	1.89	107-113	4.27	109-166	1.41	107-113	3.89	109-166	1.64	107-113	4.32	157-168	1.86
	131-137	4.80	133-167	1.92	131-137	5.24	104-171	2.54	131-137	4.92	104-171	2.64	131-137	5.31	104-171	2.74
20%	155-161	4.40	109-166	1.92	155-161	4.58	115-171	2.22	155-161	4.57	115-171	1.79	155-161	4.77	165-170	2.00
	107-113	4.30	157-168	1.88	107-113	4.34	165-170	1.67	107-113	4.15	157-168	1.71	107-113	4.35	133-167	1.91
	131-137	4.50	152-173	3.02	131-137	5.09	152-173	2.98	131-137	4.74	152-173	3.14	131-137	4.84	152-173	2.98
30%	155-161	4.24	128-172	2.75	155-161	4.52	163-173	2.76	155-161	4.38	128-172	2.84	155-161	4.37	128-172	2.69
	107-113	3.95	153-176	2.56	107-113	4.10	128-172	2.69	107-113	3.91	153-176	2.64	107-113	3.95	153-176	2.47
	131-137	4.09	152-173	2.97	131-137	5.03	152-173	2.93	131-137	4.48	152-173	3.09	131-137	4.52	152-173	2.98
40%	155-161	4.04	128-172	2.70	155-161	4.54	128-172	2.67	155-161	4.25	128-172	2.83	155-161	4.28	128-172	2.68
	107-113	3.73	153-176	2.54	107-113	4.08	163-173	2.65	107-113	3.92	153-176	2.62	107-113	3.80	153-176	2.48
	155-161	3.59	152-173	2.94	131-137	5.05	152-173	2.95	131-137	4.26	152-173	3.07	131-137	4.45	152-173	3.04
50%	131-137	3.44	128-172	2.81	155-161	4.57	128-172	2.67	155-161	4.08	128-172	2.88	155-161	4.20	128-172	2.69
	107-113	3.40	129-175	2.58	107-113	4.02	163-173	2.62	107-113	3.81	153-176	2.66	107-113	3.56	153-176	2.64
	155-161	3.64	152-173	3.16	131-127	5.04	152-173	2.94	131-137	4.16	152-173	3.14	131-137	4.32	152-173	3.03
66%	131-137	3.47	128-172	2.92	155-161	4.57	128-172	2.66	155-161	4.02	128-172	2.95	155-161	4.11	128-172	2.73
	152-173	3.16	153-176	2.95	107-113	3.99	163-173	2.59	107-113	3.68	153-176	2.77	107-113	3.41	153-176	2.71
	155-161	3.87	152-173	3.16	131-127	5.06	152-173	2.94	131-137	4.04	152-173	3.14	131-137	4.31	152-173	3.08
74%	131-137	3.52	153-176	2.95	155-161	4.55	128-172	2.67	155-161	4.00	128-172	2.94	155-161	4.07	153-176	2.78
	152-173	3.16	128-172	2.92	107-113	3.98	163-173	2.55	107-113	3.46	153-176	2.80	107-113	3.47	128-172	2.74

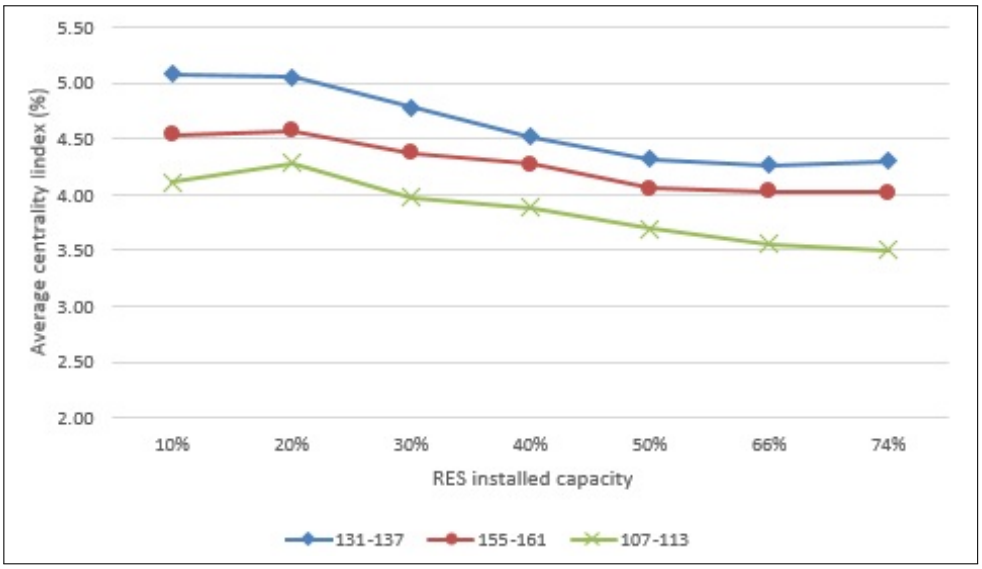

Figure 8.4: Centrality index: weighted mean of top 3 edges before storage integration

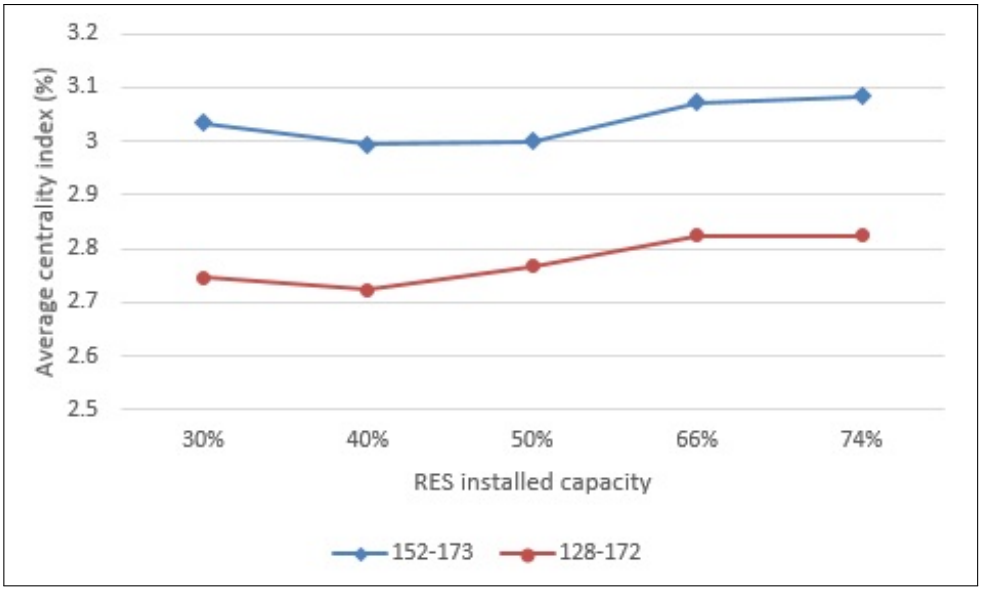

Figure 8.5: Centrality index: weighted mean of the two most significant renewable lines

With the aim of identifying the most stressed line, a ranking is provided according to the average number of time steps in which the edge reaches its capacity limit, that is $U(e)_j = 100$.

The line 132-133 carries its maximum power flow on average over four

Table 8.4: Ranking of the lines reaching their maximum capacity before storage integration

Ranking	Line	Quarters of an hour	Renewable
1	132-133	98	✗
2	117-178	77	✓
3	95-177	68	✓
4	96-180	67	✓
5	141-179	46	✓
6	156-157	39	✗
7	108-109	35	✗
8	152-173	34	✓
9	153-176	20	✓
10	165-170	17	✓
10	128-172	17	✓
11	154-156	16	✗
12	146-150	15	✗
13	130-132	12	✗
14	117-118	11	✗
15	143-179	9	✓
15	158-169	9	✓
16	98-102	7	✗
17	118-122	6	✗
18	129-175	5	✓
19	113-170	3	✓
20	119-140	2	✗
21	93-177	1	✓
21	99-100	1	✗

days for 98 quarters of hour out of 384, that is around one-fourth the time in question. The scenarios with low RES capacity, i.e. 10% and 20%, are the most influential, with 133 and 139 out of 384 respectively.

Then, there are four lines linked to a wind farm; of course, their average overload duration is valued as a mean over only the scenarios where the farms are added, in which their overload duration tends to increase. Fig.8.6 shows the overload duration curve for these edges in Winter in two different cases. As can be observed, the greater RES installed capacity determines a higher utilization of the lines, especially for 96-180 and 95-177, whose, from having the maximum values equal to 82.7% and 93% respectively, become the most overloaded during the day.

The next step is the integration of storage systems in our grid in order to reduce the energy curtailment and try avoiding the lines congestion.

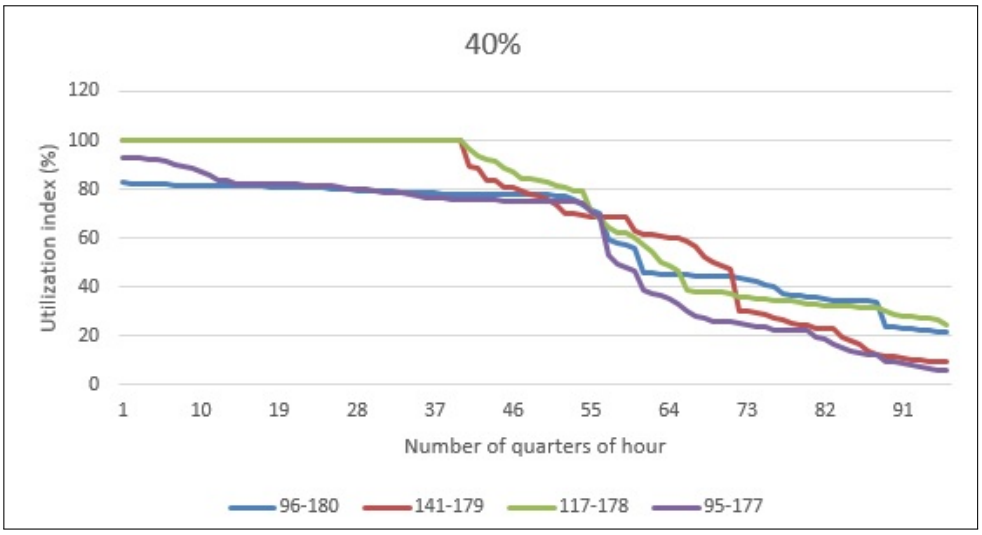

(a) 40% of RES installed capacity

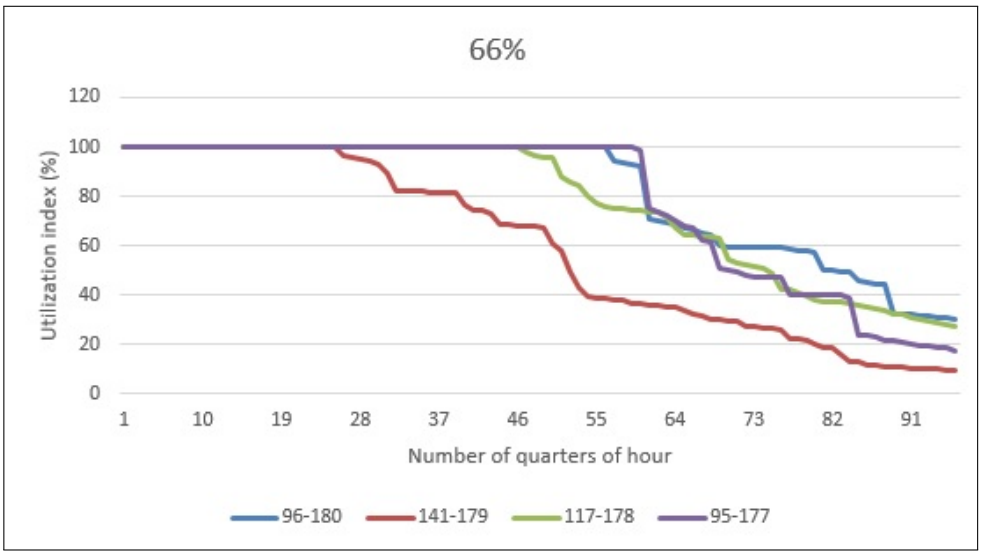

(b) 66% of RES installed capacity

Figure 8.6: Winter: overload duration curve for the most stressed four renewable lines with two different percentage of RES installed capacity

8.3.3 Results with storage

Looking at the ranking in Tab.8.4, one can see that 13 lines out of 24 are linked to wind farms; anyway, since there are three cases in which two lines start from the same one, only 10 buses are identified as the most interesting ones. According to the capacity of the line, as explained in Sec.4.5.1, Tab.8.5 summaries the characteristics of the storages added to the grid. For both

kinds of devices, the DoD and the charge/discharge efficiency are estimated to be equal to 80% and 87% respectively. As previously stated in Sec.3.4, all storage devices are energy intensive applications, according to this thesis work's scope.

Table 8.5: Storage systems' characteristics

Line's capacity	**$SoC_{b,max}$**	**$ch_{b,max}$**	**K**	**$SoC_{b,min}$**	**$SoC_{b,0}$**	**Quantity**
MW	**MWh**	**MW**	**h**	**MWh**	**MWh**	
131	131	19	6.89	27	27	4
375	375	75	6.69	75	75	6

Moreover, since the data analysis takes a considerable time because only partially automated by means of Excel Macros, the possible effects of storage systems introduction are investigated only in two cases, the ones with the renewable installed capacity equal to 40% and 66% of the winter global load demands (Tab.8.6).

Table 8.6: Scenarios with storage systems

Renewable installed capacity (MW)	3 960	5 910
% of winter demand	40	66
% of total generation capacity	28.1	36.7
Generation (MW)	14 175	16 075
Thermal (MW)	9 315	9 315
Hydro (MW)	900	900
Solar-PV (MW)	660	660
Wind (MW)	3 300	5 250
EESS		
Energy capacity (MWh)	2 774	2 774
Power capacity (MW)	412	412

The batteries are added following the policies explained in Sec.4.5.2, thereby getting three different grid structures as summarises in Tab.8.7.

First of all, we value the reduction in energy curtailment. As can be seen in Tab.8.8, with 40% of RES capacity, there is no difference between the various siting policies and it is reduced by 27.36% (4 615 MWh); whereas, with 66%, the random siting provides the best result, -21.87% (11 463 MWh). Anyway, it is worth to note that if on the one hand in Winter this policy guarantees the exploitation of extra 183.8 MWh from RES, that is +1.3%, on the other one in Summer the siting policy that follows the ranking is the

Table 8.7: Integration of batteries: siting of energy storage devices , according to three different policies

Type of battery (MWh - MW)	**Random to bus**	**Ranking to bus**	**Wind to bus**
131-19	178	178	178
131-19	118	177	177
131-19	150	180	180
131-19	122	179	179
375-56	133	133	169
375-56	173	173	173
375-56	157	157	172
375-56	109	109	175
375-56	132	170	170
375-56	156	176	176

best one. In this case, indeed, the grid is able to use 163.3 MWh more than in the other ones, that is +6.3%.

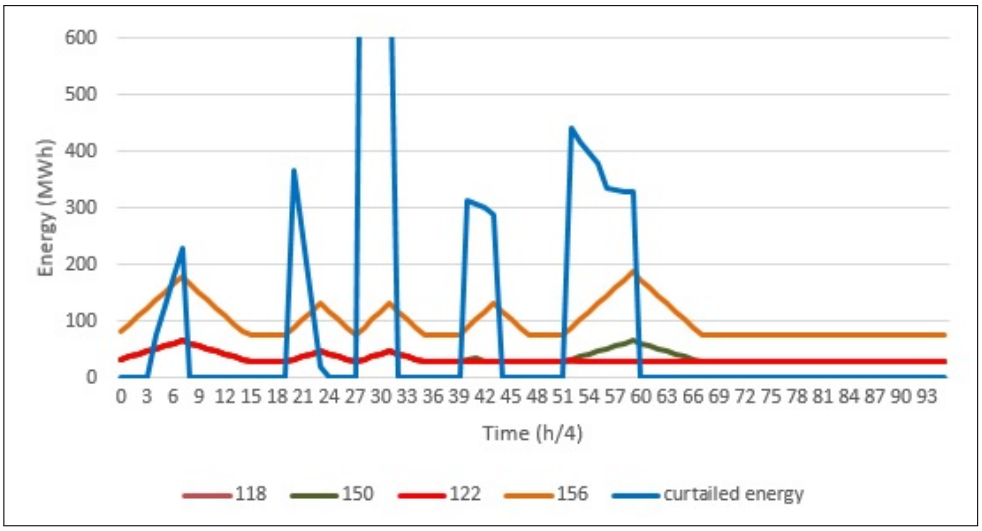

Figure 8.7: 66% Summer Random: state of charge of different storages

In Fig.8.7, the SoC of different storages are shown: during the curtailment peaks between the time steps 40-43 and 52-59, the batteries linked to bus 122 and 118 are not exploited by the grid, while around 109 MW produced by the close wind farm 193 are curtailed. A "screenshot" of the power flowing on the area of interest at the time step 55 is represented in Fig.8.8. The line 178-117 is carrying its maximum flow (131MW) and the

Table 8.8: Curtailed energy after the introduction of batteries by following three policies

40%	**Curt**	**RANDOM**	**RANKING**	**WIND**
	MWh	**MWh**	**MWh**	**MWh**
W	4 422.2	2 899.6	2 899.6	2 899.6
SP	1 257.5	758.9	758.9	758.9
SU	80.8	0	0	0
AU	11 106.9	8 594	8 594	8 594
Total (MWh)	16 867.4	12 252.5	12 252.5	12 252.5
Reduction %		-27.36	-27.36	-27.36
66%	**Curt**	**RANDOM**	**RANKING**	**WIND**
	MWh	**MWh**	**MWh**	**MWh**
W	17 003.3	13 793.5	13 977.3	13 977.3
SP	4 134.7	2 898.5	2 898.5	2 898.5
SU	5 241.1	2 604	2 440.7	2 461.9
AU	26 028.9	21 649.5	21 649.5	21 665.4
Total (MWh)	52 408	40 945.5	40 966	41 003.1
Reduction %		-21.87	-21.83	-21.76

area is importing 931.5 MW from the North, while only 16.5 MW are exporting towards Area 1. Moreover, the conventional plant 15 is producing 19.6 MW more than its lower limit and, by comparing the same time step in "ranking" and "random", which differ for the position of 5 batteries, we notice that the curtailment at wind farms 192, 194 and 195 increases.

The following tables 8.9, 8.10 and 8.11 summarize the exploitation of the batteries by using three parameters already defined in Sec.8.1.3: the number of quarters of hour during which $SoC_{b,j} > SoC_{b,min}$, the average of the maximum energy stored SoC_{av} and the average of the maximum power injected or extracted ch_{av}, both valued above four days.

As can be observed, the batteries' exploitation increases considerably from the first scenario to the second one, with an average utilization that rises from 91 to 234 in terms of time steps.

In general, the different siting doesn't affect significantly the devices' utilization and the last one is not always coherent with the ranking of the most stressed lines. For instance, even if line 132-133 is the most overloaded, when a battery is added to bus 133, it stores up energy for less then 20% of the time considered. Considering the buses with wind farms, the batteries linked to node 178, 179 and 173 are the most used during the four days, while the ones to node 177 and 180 are the least exploited.

In the first scenario, batteries' power capacity is not always used completely, since in Summer the energy curtailment is quite limited; moreover,

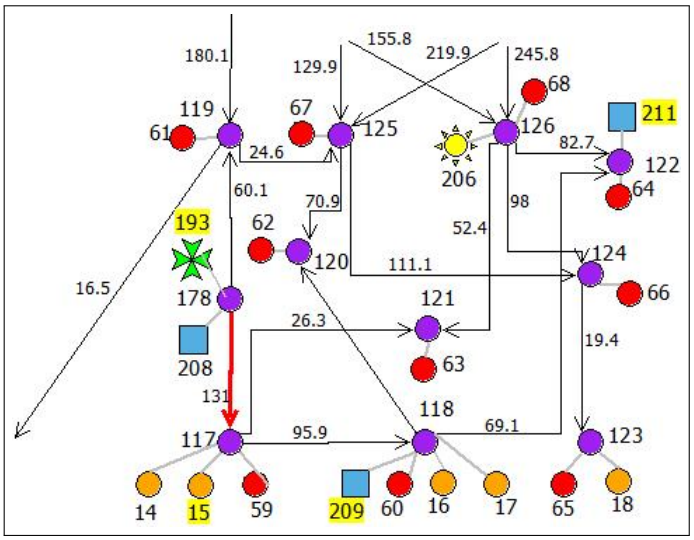

Figure 8.8: 66% Summer Random: power flow at j=55

Table 8.9: Summary table about batteries' exploitation when "random" policy is applied for siting

	40%				66%			
	h/4	**SoC_{av}**		**ch_{av}**	**h/4**	**SoC_{av}**		**ch_{av}**
		MWh	**%**	**MW**		**MWh**	**%**	**MW**
178	154	72.0	55.0	19.0	256	102.7	78.4	19.0
118	84	70.9	54.1	19.0	200	91.0	69.5	19.0
150	109	77.4	59.1	19.0	227	92.2	70.4	19.0
122	72	69.7	53.2	19.0	208	91.2	69.6	19.0
133	63	190.5	50.8	42.0	231	267.0	71.2	56.0
173	101	218.0	58.1	56.0	238	265.5	70.8	56.0
157	83	204.5	54.5	56.0	241	267.0	71.2	56.0
109	66	190.6	50.8	42.0	222	263.7	70.3	56.0
132	69	198.2	52.9	44.8	232	267.0	71.2	56.0
156	90	208.0	55.5	56.0	238	267.0	69.9	56.0

the maximum states of charge are never reached. When the "ranking" siting policy is adopted, the device linked to bus 178 accumulates 125 MWh, that is 95% of it capacity, which results in the highest value of SoC_{av} in percentage, 61.8%.

As the curtailment increases, all batteries fully exploit their power limits, the SoC_{av} always exceeds 70% of the energy capacity and in Winter and Autumn the maximum state of charge is often reached. Despite of the siting policy, one can see an uniform behaviour at equal characteristics.

Table 8.10: Summary table about batteries' exploitation when "ranking" policy is applied for siting

	40%				66%			
	h/4	**SoC_{av}**		**ch_{av}**	**h/4**	**SoC_{av}**		**ch_{av}**
		MWh	**%**	**MW**		**MWh**	**%**	**MW**
178	163	80.9	61.8	19.0	258	102.7	78.4	19.0
177	63	66.2	50.5	14.3	220	91.0	69.5	19.0
180	63	66.2	50.5	14.3	223	92.2	70.4	19.0
179	144	77.7	59.3	19.0	254	100.2	76.5	19.0
133	68	197.0	52.5	45.0	230	267.0	71.2	56.0
173	100	218.0	58.1	56.0	239	265.5	70.8	56.0
157	84	204.5	54.5	56.0	242	267.0	71.2	56.0
109	64	190.5	50.8	42.0	225	263.7	70.3	56.0
170	74	201.0	53.6	56.0	236	267.0	71.2	56.0
176	90	210.6	56.2	56.0	237	267.0	71.2	56.0

Table 8.11: Summary table about batteries' exploitation when "wind" policy is applied for siting

	40%				66%			
	h/4	**SoC_{av}**		**ch_{av}**	**h/4**	**SoC_{av}**		**ch_{av}**
		MWh	**%**	**MW**		**MWh**	**%**	**MW**
178	158	75.8	57.9	19.0	259	102.7	78.4	19.0
177	63	66.2	50.5	14.3	232	93.2	71.2	19.0
180	63	66.2	50.5	14.3	225	93.0	71.0	19.0
179	143	77.6	59.2	19.0	265	102.3	78.1	19.0
173	100	218.0	58.1	56.0	240	267.0	71.2	56.0
170	65	190.7	50.8	42.0	231	267.0	71.2	56.0
176	90	210.6	56.2	56.0	239	267.0	71.2	56.0
172	73	199.7	53.3	56.0	221	262.0	69.9	56.0
169	84	204.5	54.5	56.0	238	267.0	71.2	56.0
175	72	197.8	52.7	43.2	226	262.0	69.9	56.0

The storages at buses 178 and 179 (when installed) continue to be the most used, both in terms of quarters of hour and capacities.

It is worth to notice what happens in the summer day during the time steps 40-43 and 52-59, by comparing "ranking" and "wind" scenarios, which differ for the siting of three 375 MWh batteries; in particular, in the first one they are linked to buses 133, 157, 109, while in the second one to buses 169, 172, 175. Even if the total curtailment is almost the same, with a difference

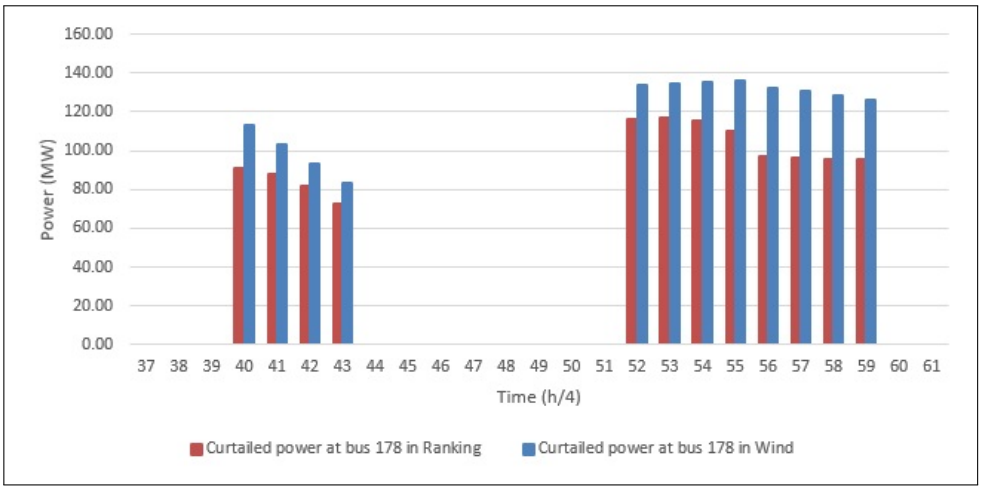

(a) Bus 178

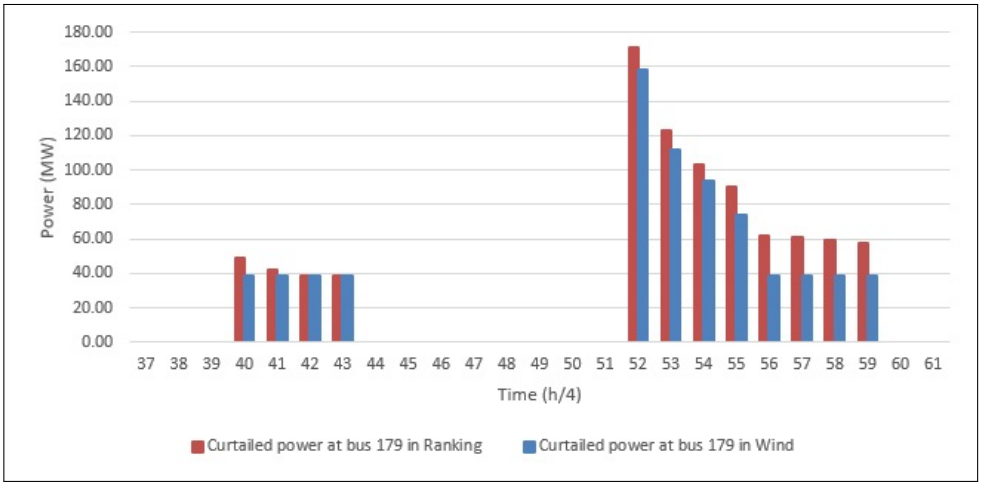

(b) Bus 179

Figure 8.9: Comparison of the curtailed power at bus 178 and 179 between "wind" and "ranking"

smaller than 9 MW per quarter of hour, the different flows distribution involve significantly the wind farms at buses 178 and 179. The exploitation of the former in "wind" is lower than in "ranking", with an increase of the curtailed power of 22.8 MW on average, while the latter's one is higher, with a reduction of the curtailment of 12.6 MW per time step, Fig.8.9.

We conclude the analysis of storages' behaviour reporting a graph that shows their effects on the power curtailment. The load curve and the "adjusted" renewable production (including the minimum technical output fo conventional generators) are the same in both Fig.8.10a and Fig.8.10b (left y axis), while the curtailment decreases thanks to the batteries, whose total

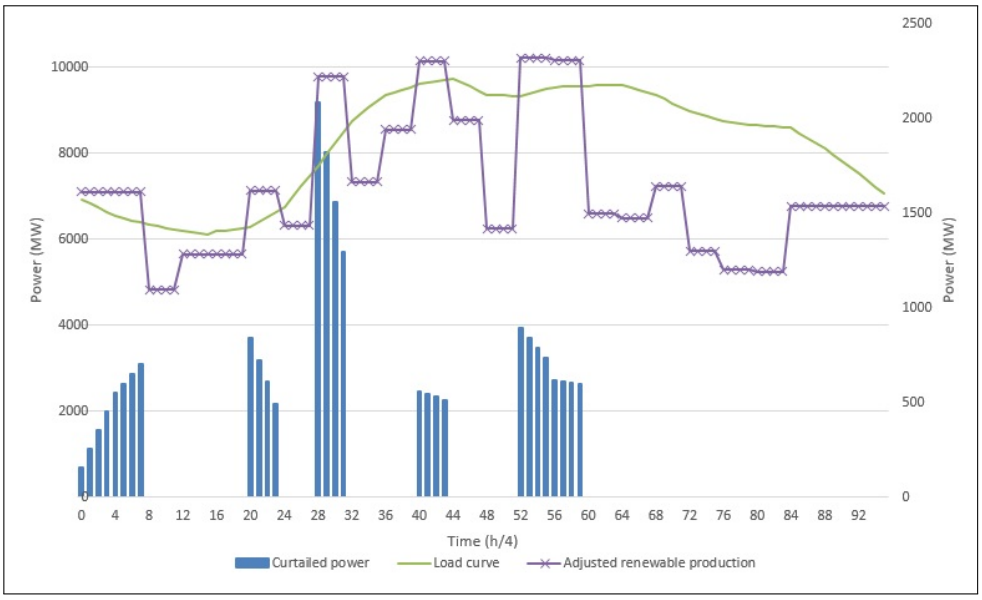

(a) Before batteries' introduction

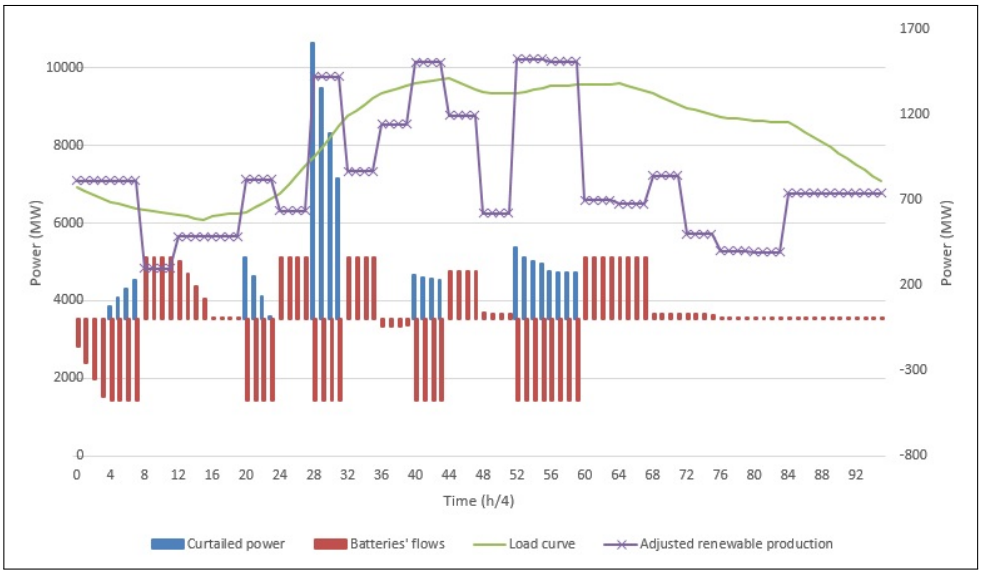

(b) After batteries' introduction

Figure 8.10: Effects of batteries on power curtailment

flows are added in the latter one (both on the right y axis). One can see that these devices are charged when the available production is higher than load demand, while they discharge as soon as there is the opportunity to use the stored energy to limit the supply from conventional plants.

Since the ranking in Tab.8.4 is drawn up by considering all scenarios,

from 10% to 74% of RES installed capacity, while now we take into account only the scenario with 40% and 66% of renewable power, the ranking is redrafted as follows, Tab.8.12.

In this table, one can compare the overload average duration for each line without storage and by following three different policies for the siting, and a ✓indicates if a battery is linked to one of the end-vertexes of the edge.

Overall, there are no relevant differences that could be directly attributed to the siting policies, given that the average overload duration remains almost the same.

Table 8.12: Ranking of the lines reaching their maximum capacity before storage integration and by following different policies for the storages' siting

Line	**No storage**	**Random**		**Ranking**		**Wind**	
117-178	81	90	✓	87	✓	86	✓
132-133	80	67	✓	76	✓	54	
95-177	62	68		68	✓	66	✓
96-180	56	56		54	✓	54	✓
141-179	52	60		60	✓	59	✓
152-173	35	30	✓	31	✓	35	✓
156-157	23	25	✓	22	✓	20	
108-109	21	28	✓	34	✓	18	
153-176	18	18		15	✓	9	✓
128-172	17	20		17		18	✓
165-170	17	16		13	✓	15	✓
130-132	12	16	✓	9		10	
154-156	12	11	✓	10		10	
117-118	11	14	✓	17		21	
158-169	9	8		8		4	✓
146-150	8	5	✓	5		5	
129-175	3	1		3		3	✓
113-170	2	3		6	✓	6	✓
118-122	1	1	✓	1		1	
143-179	1	2		2	✓	5	✓
Av. dur.	26	27		27		25	

Anyway, with a further examination, we can point out an interesting example of the effects of the introduction of storage in terms of transmission congestions resolution.

Area 1 has a surplus of cheap generation that is exported toward Area 2 and 3 through the edges 115-133 and 113-170; then, focusing on the first zone, line 132-133 carries this power, together with the one coming from the neighbouring plants, both conventional and renewable, to the central area.

Since this line has a capacity of only 375 MW, despite of its strategical position, it's the most stressed above all the grid and among the most influenced by storage introduction, with a decreasing of the overload up to -33% when batteries are added close to wind farms.

In particular, in summer with 66% of renewable capacity, the overload is reduced from 20 time steps to 4, that is -80%. Between time steps 32-36 and 60-71, indeed, this edge is positively influenced by the discharge of storages, without reaching the capacity limit, as one can see in Fig.8.11.

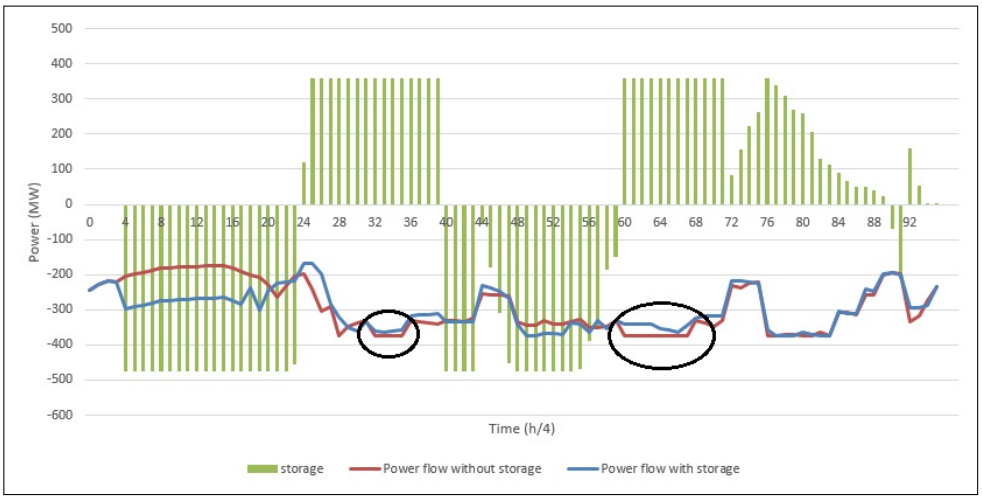

Figure 8.11: Chronological power flow on line 132-133 without and with storage, and storage behaviour, in Summer 66% "wind" scenario.

Finally, a centrality analysis is performed by means of the metrics already defined in Sec.8.1.3 and used in Sec.8.3.2. Anyway, since it is defined as the ratio between the flow on the line and the total flow on the grid, where the latter is far greater than the former, this index is not expected to be significantly affected by the introduction of the storage, whatever siting policy is followed. Fig.8.12 shows two different comparison: the first one is between a scenario without storage and the same one after the batteries introduction; the second one focuses only on renewable lines.

One can see that there are four edges with a high value {131-137, 155-161, 107-113, 132-133} which means that this small portions of lines carries a significant part of the global flow (around 16%), followed by an almost linear trend, which means it is quite difficult to point out very critical lines, as it should be in a meshed network in order to avoid cascading failure.

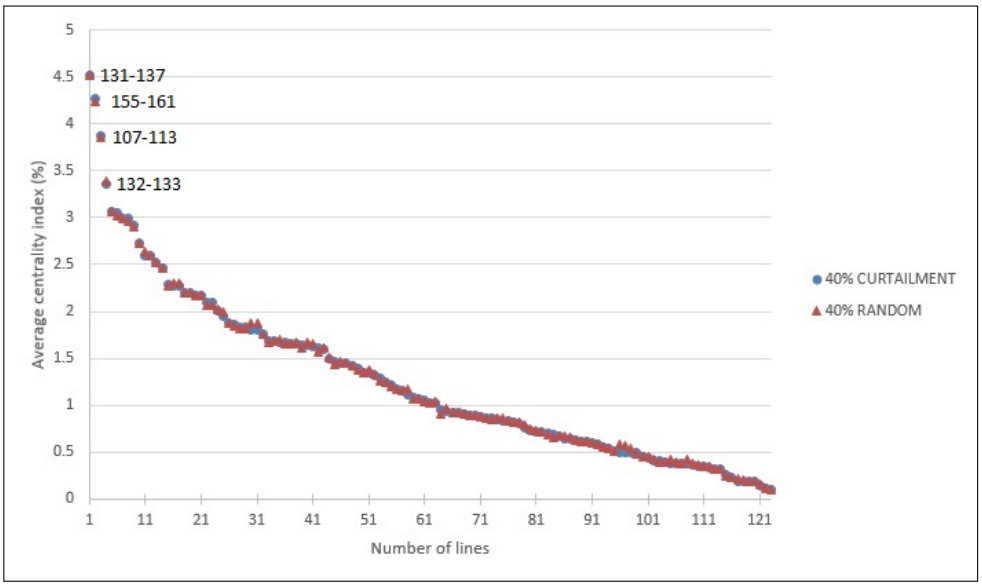

(a) Comparison of the overall trend of centrality index between a scenario without storage and after batteries' introduction

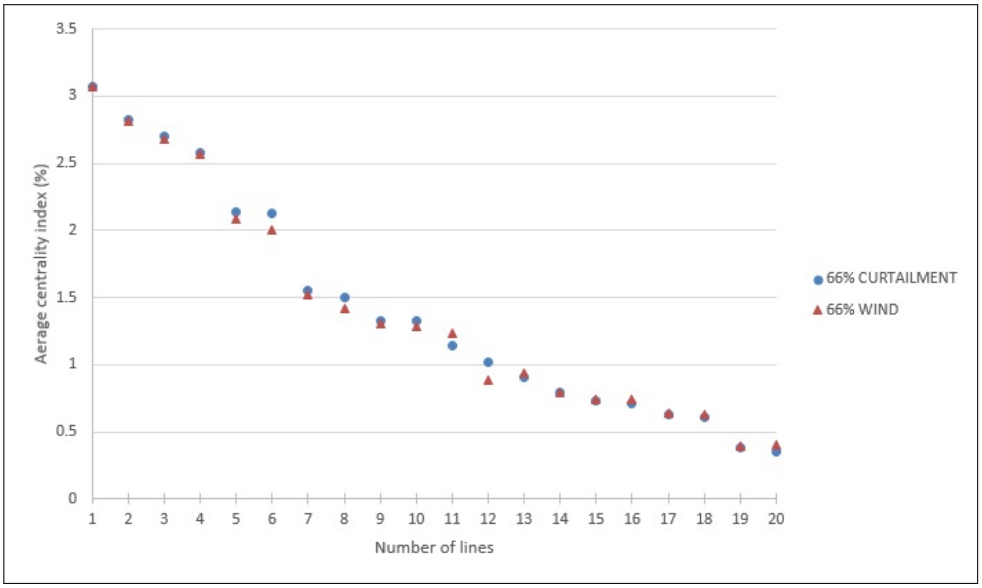

(b) Comparison of the average centrality index of renewable lines without and with storage, added near wind farms.

Figure 8.12: Centrality index: comparison before and after batteries' introduction

9

Conclusions and future work

9.1 Summary

As a results of the European de-carbonisation energy policy, managing a high amount of varying power supply from renewable sources is a new challenge for power grids. An optimization tool has been developed to model a power system as a weighted graph by a topological point of view, and a DC power flow was run above it, with the aim of minimizing the production costs over a determined time horizon. We used a modified version of IEEE-RTS 96 as test case, adding some renewable plants and then, in order to reduce the power curtailment, some electrochemical storage systems. These ones were introduced into the grid by following three siting policies and their effects are valued by different point of view:

- better exploitation of RES sources;
- resolution of overloads of lines;
- re-distribution of power flows above the graph.

9.2 Discussion

The developed software guarantees the optimal solution of our problem, respecting all the linear constrains of the model, with good performances in term of run-time and use of memory. They both increase linearly with the number of nodes, that means the software could be used for investigating the behaviour of real grid with much more nodes, such as a part of the European HV network, by simply enhancing the computational capabilities of hardware.

The power curtailment increases by varying the percentage of RES and when it becomes quite high, it affects also PV plants, as was to be expected, according to the cost coefficients. The most involved are the ones in Area

3, since it has no way to export its extra production and it imports the cheaper wind power from farms 184 and 185. The introduction of some batteries allows the grid to store energy during off-peak period, or when the renewable availability is excessive, and use it to limit the supply from conventional plants at a later time. This benefit is clearly shown in Fig.8.10: the charge of these devices corresponds to a lower curtailment and their discharge occurs as soon as there is a decrease in wind production.

In this way, the reduction of power curtailment reaches 4 614.9 MW in four days, that is -27.4% when the RES installed capacity is equal to 40% of winter peak demand, and 11462.5 MW, -21.9%, when the RES capacity is 66%. In the first scenario, the different siting policies do not influence the results, while in the second one, since flows are higher, transmission congestions can impede the optimal exploitation of batteries (e.g. Fig.8.8), even in a different Area, as it happens in the summer day. For instance, what occurs at buses 178, Fig.8.9a, can be attributed to the removal of a 375 MWh storage from bus 109, that implies in "wind" scenario higher flow from the North to the South of Area 1, reducing the import of renewable power from Area 2 and, in particular, from the wind farm at bus 178.

At the same time, moving a battery from bus 157 to 169, near a wind farm, reduces the curtailment at bus 179 (Fig.8.9b), since the surplus of power at node 169 can be stored, limiting the export from North to South in Area 3 and allowing a better utilization of the local renewable production.

If on one hand the different policies of siting have not significantly influenced the average overload duration of the lines, on the other one this work has proved that the storage introduction can avoid the congestion of a critical corridor. By comparing power flows on line 132-133 in Fig.8.11, indeed, one can see that the batteries discharge prevents the edge reaching its capacity limit in many time steps.

This concept is important also by an economical point of view. The conventional generators are maintained, indeed, at their minimal technical levels as long as it is possible to dispatch the renewable power to fulfil the load demand; however, in case of congestion, it can happen that some conventional plants are required to produce more, even if there is a surplus of RES production (Fig.8.8). Since in this thesis, generators' ramp rates haven't been taken into account, the cheap coal plants are the ones called to increase their output, but, in a real system, this would involve other more expensive mitigation measures, such as generation re-distribution and start-up of a fast unit.

Finally, a centrality analysis shows that, even with the introduction of batteries, the lines that carries the highest portions of the global flow are still the same. These edges are the ones transmitting the production of cheap plants, e.g. nuclear and hydro, from the North to the South of each

area, where there are more expensive plants and more loads. With the growing of RES capacity the conventional production is substituted by the renewable one, which means that the power carried by the aforementioned edges decreases (Fig.8.4), while flows above the ones linked to a wind farms increase (Fig.8.5).

9.3 Future work

Further research can be conducted based on the work presented in this thesis. First of all, a software to represent the power flows above all the grid could be developed to visualize the situation of the grid, together with a program to make the data analysis automated and faster.

A sensitivity analysis could be the best approach for storages' siting, with the purpose to place them where they could guarantee greater benefits for the grid in term of relief of congestions and/or reduction of curtailment. An economic evaluation of these benefits should be compared with the investment costs of such kind of project, also investigating how far away these costs are from being economically profitable. In addition, it could be considering the possibility to introduce devices with a smaller discharge duration and a higher power capacity.

Moreover, it could be worth to investigate if a topological reconfiguration of the grid, adding or replacing edges, could allow a better exploitation both of the RES sources and the storage.

Last but not least, the model should take into account also other parameters, such as market price, and not only the possibility of power curtailment, but also load shedding. In this scenario, a probabilistic model could be useful to account for all possible conditions in terms of supply-demand and contingencies, such as outages and errors in both load demand and renewable production forecasts.

10

Appendix

10.1 Data input

The new version of the IEEE RTS-96 is modelled as described in Sec.4.4, adding renewable plants and storage as explained in Sec.7.3 and Sec.4.5.2. For each scenario, an input text file is written according to the following criteria:

- a "summarizing" line: number of time periods, daily maximum load demand, total number of nodes, number of conventional plants, number of renewable plants, number of loads, numbers of storage systems, duration of each step, charge and discharge efficiency of storages.

  ```
  96 9716 218 42 27 51 10 0,25 0,87 0,87
  ```

- The keyword "generators" introduces the grid description: lower and upper power generation limits, cost coefficient, T or H to distinguish between thermal and hydro plants. In this way, the hydro plants are decommissioned if the load demand is lower than 70% of the daily maximum peak.

```
generators
16,00 40,00 70,00 T
76,00 152,00 55,00 T
16,00 40,00 70,00 T
76,00 152,00 55,00 T
120,00 300,00 60,00 T
236,40 591,00 55,00 T
24,00 60,00 80,00 T
77,50 155,00 45,00 T
77,50 155,00 45,00 T
280,00 400,00 35,00 T
280,00 400,00 35,00 T
0,00 300,00 10,00 H
155,00 310,00 45,00 T
175,00 350,00 40,00 T
16,00 40,00 70,00 T
76,00 152,00 55,00 T
16,00 40,00 70,00 T
76,00 152,00 55,00 T
120,00 300,00 60,00 T
236,40 591,00 55,00 T
24,00 60,00 80,00 T
```

```
77,50 155,00 45,00 T
77,50 155,00 45,00 T
280,00 400,00 35,00 T
280,00 400,00 35,00 T
0,00 300,00 10,00 H
155,00 310,00 45,00 T
175,00 350,00 40,00 T
16,00 40,00 70,00 T
76,00 152,00 55,00 T
16,00 40,00 70,00 T
76,00 152,00 55,00 T
120,00 300,00 60,00 T
236,40 591,00 55,00 T
24,00 60,00 80,00 T
77,50 155,00 45,00 T
77,50 155,00 45,00 T
280,00 400,00 35,00 T
280,00 400,00 35,00 T
0,00 300,00 10,00 H
155,00 310,00 45,00 T
175,00 350,00 40,00 T
```

- "consumers" and "totloads" are followed by the total load demand for each quarter-hour.
- "perloads" means the percentage of load assumed for each bus (See Sec.4.4).

```
consumers 6741
totloads 6981
6926 7221
6828 7461
6730 7701
6633 7964
6535 8227
6484 8490
6433 8753
6382 8902
6331 9051
6297 9200
6262 9350
6228 9411
6194 9472
6160 9534
6126 9595
6091 9625
6181 9656
6205 9686
6229 9716
6253 9627
6278 9538
6394 9449
6509 9360
6625 9351
```

9342	7219
9334	7073
9325	perloads
9378	1,27
9430	1,13
9483	2,10
9536	0,87
9542	0,83
9549	1,60
9555	1,47
9562	2,00
9568	2,03
9575	2,27
9581	3,10
9588	2,27
9528	3,70
9468	1,17
9408	3,90
9348	2,13
9252	1,50
9156	1,27
9060	1,13
8963	2,10
8904	0,87
8845	0,83
8785	1,60
8726	1,47
8705	2,00
8683	2,03
8662	2,27
8640	3,10
8627	2,27
8613	3,70
8600	1,17
8587	3,90
8463	2,13
8339	1,50
8215	1,27
8090	1,13
7946	2,10
7801	0,87
7657	0,84
7512	1,60
7366	1,47

```
2,00                    3,70
2,03                    1,17
2,27                    3,90
3,10                    2,13
2,27                    1,50
```

- "rgenerators" introduces the properties of the renewable plants added to the grid: curtailment cost, cost coefficients, installed capacity of each farms and S or W, solar or wind respectively.
- Both the wind and solar-PV generation in p.u. per each periods are listed, preceded by the keywords "wind" and "solar". In this way, the power potentially available $P_{r,av}$ per each renewable plant is calculated (See Eq.(5.2b)).

```
rgenerators             55 S
300                     55 S
0,5                     55 S
1,25                    wind
350 W                   0,43
350 W                   0,43
350 W                   0,43
350 W                   0,43
350 W                   0,43
350 W                   0,43
350 W                   0,43
350 W                   0,43
350 W                   0,00
350 W                   0,00
350 W                   0,00
350 W                   0,00
350 W                   0,16
350 W                   0,16
350 W                   0,16
55 S                    0,16
55 S                    0,16
55 S                    0,16
55 S                    0,16
55 S                    0,16
55 S                    0,43
55 S                    0,43
55 S                    0,43
55 S                    0,43
```

0,27	0,43
0,27	0,43
0,27	0,43
0,27	0,43
0,92	0,16
0,92	0,16
0,92	0,16
0,92	0,16
0,43	0,08
0,43	0,08
0,43	0,08
0,43	0,08
0,64	0,08
0,64	0,08
0,64	0,08
0,64	0,08
0,92	0,37
0,92	0,37
0,92	0,37
0,92	0,37
0,64	0,37
0,64	0,37
0,64	0,37
0,64	0,37
0,16	0,37
0,16	0,37
0,16	0,37
0,16	0,37
0,92	solar
0,92	0,00
0,92	0,00
0,92	0,00
0,92	0,00
0,92	0,00
0,92	0,00
0,92	0,00
0,27	0,00
0,27	0,00
0,27	0,00
0,27	0,00
0,27	0,00
0,27	0,00
0,27	0,00
0,27	0,00

0,00	0,75
0,00	0,75
0,00	0,75
0,00	0,75
0,00	0,50
0,05	0,50
0,05	0,50
0,05	0,50
0,05	0,35
0,10	0,35
0,10	0,35
0,10	0,35
0,10	0,20
0,20	0,20
0,20	0,20
0,20	0,20
0,20	0,10
0,35	0,10
0,35	0,10
0,35	0,10
0,35	0,05
0,50	0,05
0,50	0,05
0,50	0,05
0,50	0,00
0,75	0,00
0,75	0,00
0,75	0,00
0,75	0,00
0,85	0,00
0,85	0,00
0,85	0,00
0,85	0,00
0,90	0,00
0,90	0,00
0,90	0,00
0,90	0,00
0,85	0,00
0,85	0,00
0,85	0,00
0,85	

- "storage" introduces the properties of each storage system: $SoC_{b,in}$, that is the state of charge at the beginning of the first quarter-hour,

$SoC_{b,max}$, $SoC_{b,min}$.

```
storage
27 131 27
27 131 27
27 131 27
27 131 27
75 375 75
75 375 75
75 375 75
75 375 75
75 375 75
75 375 75
```

- Finally, "network" introduces the edges, both the real and the dummy ones: end-vertices, reactance, capacity.

```
network
93 94 0,0140 131
93 97 0,0850 131
94 98 0,1920 131
95 101 0,0310 131
95 116 0,0840 300
96 101 0,1040 131
97 102 0,0880 131
98 102 0,0610 131
99 100 0,0610 131
99 119 0,1610 131
100 101 0,1650 131
100 102 0,1650 131
101 103 0,0840 300
101 104 0,0840 300
102 103 0,0840 300
102 104 0,0840 300
103 105 0,0480 375
103 106 0,0420 375
104 105 0,0480 375
105 131 0,0750 375
106 108 0,0590 375
107 108 0,0170 375
107 113 0,0245 750
107 116 0,0520 375
108 109 0,0260 375
108 111 0,0230 375
109 110 0,0140 375
110 113 0,0130 750
111 112 0,0200 750
112 115 0,0110 750
113 114 0,0680 375
115 133 0,0740 375
117 118 0,0140 131
117 121 0,0850 131
118 120 0,1270 131
118 122 0,0192 131
119 125 0,1190 131
119 140 0,0840 300
120 125 0,1040 131
121 126 0,0880 131
122 126 0,0610 131
123 124 0,0610 131
124 125 0,1650 131
124 126 0,1650 131
125 127 0,0840 300
125 128 0,0840 300
126 127 0,0840 300
126 128 0,0840 300
127 129 0,0480 375
127 130 0,0420 375
128 129 0,0480 375
130 132 0,0590 375
131 132 0,0170 375
```

131 137 0,0245 750
131 140 0,0520 375
132 133 0,0260 375
132 135 0,0230 375
133 134 0,0140 375
134 137 0,0130 750
135 136 0,0200 750
136 139 0,0110 750
137 138 0,0680 375
141 142 0,0140 131
141 145 0,0850 131
142 144 0,1270 131
142 146 0,1920 131
143 149 0,1190 131
143 164 0,0840 300
144 149 0,1040 131
145 150 0,0880 131
146 150 0,0610 131
147 148 0,0610 131
148 149 0,1650 131
148 150 0,1650 131
149 151 0,0840 300
149 152 0,0840 300
150 151 0,0840 300
150 152 0,0840 300
151 153 0,0480 375
151 154 0,0420 375
152 153 0,0480 375
154 156 0,0590 375
155 156 0,0170 375
155 161 0,0245 750
155 164 0,0520 375
156 157 0,0260 375
156 159 0,0230 375
157 158 0,0140 375
158 161 0,0130 750
159 160 0,0200 750
160 163 0,0110 750
161 162 0,0680 375
163 165 0,0090 542
0 93 0,0001 40
1 93 0,0001 152
93 42 0,0001 800
2 94 0,0001 40
3 94 0,0001 152
94 43 0,0001 800
95 44 0,0001 800
96 45 0,0001 800
97 46 0,0001 800
98 47 0,0001 800
4 99 0,0001 300
99 48 0,0001 800
100 49 0,0001 800
101 50 0,0001 800
102 51 0,0001 800
105 52 0,0001 800
5 105 0,0001 591
106 53 0,0001 800
107 54 0,0001 800
6 107 0,0001 60
7 107 0,0001 155
108 55 0,0001 800
8 108 0,0001 155
110 56 0,0001 800
9 110 0,0001 400
111 57 0,0001 800
112 58 0,0001 800
10 113 0,0001 400
11 114 0,0001 300
12 115 0,0001 310
13 115 0,0001 350
14 117 0,0001 40
15 117 0,0001 152
117 59 0,0001 800
16 118 0,0001 40
17 118 0,0001 152
118 60 0,0001 800
119 61 0,0001 800
120 62 0,0001 800
121 63 0,0001 800
122 64 0,0001 800
18 123 0,0001 300
123 65 0,0001 800
124 66 0,0001 800
125 67 0,0001 800
126 68 0,0001 800
129 69 0,0001 800
19 129 0,0001 591

130 70 0,0001 800
131 71 0,0001 800
20 131 0,0001 60
21 131 0,0001 155
132 72 0,0001 800
22 132 0,0001 155
134 73 0,0001 800
23 134 0,0001 400
135 74 0,0001 800
136 75 0,0001 800
24 137 0,0001 400
25 138 0,0001 300
26 139 0,0001 310
27 139 0,0001 350
28 141 0,0001 40
29 141 0,0001 152
141 76 0,0001 800
142 77 0,0001 800
30 142 0,0001 40
31 142 0,0001 152
143 78 0,0001 800
144 79 0,0001 800
145 80 0,0001 800
146 81 0,0001 800
147 82 0,0001 800
32 147 0,0001 300
148 83 0,0001 800
149 84 0,0001 800
150 85 0,0001 800
153 86 0,0001 800
33 153 0,0001 591
154 87 0,0001 800
155 88 0,0001 800
34 155 0,0001 60
35 155 0,0001 155
156 89 0,0001 800
36 156 0,0001 155
158 90 0,0001 800
37 158 0,0001 400
159 91 0,0001 800
160 92 0,0001 800
38 161 0,0001 400
39 162 0,0001 300
40 163 0,0001 310
41 163 0,0001 350
109 166 0,0525 375
114 166 0,0525 375
133 167 0,0525 375
138 167 0,0525 375
157 168 0,0525 375
162 168 0,0525 375
139 169 0,0520 375
158 169 0,0520 375
113 170 0,0485 375
165 170 0,0485 375
104 171 0,0485 375
115 171 0,0485 375
128 172 0,0485 375
139 172 0,0485 375
152 173 0,0435 375
163 173 0,0435 375
105 174 0,0435 375
115 174 0,0435 375
129 175 0,0435 375
139 175 0,0435 375
153 176 0,0435 375
163 176 0,0435 375
93 177 0,1055 131
95 177 0,1055 131
117 178 0,1055 131
119 178 0,1055 131
141 179 0,1055 131
143 179 0,1055 131
94 180 0,0635 131
96 180 0,0635 131
181 166 0,0001 350
182 167 0,0001 350
183 168 0,0001 350
184 169 0,0001 350
185 170 0,0001 350
186 171 0,0001 350
187 172 0,0001 350
188 173 0,0001 350
189 174 0,0001 350
190 175 0,0001 350
191 176 0,0001 350
192 177 0,0001 350
193 178 0,0001 350

```
194 179 0,0001 350
195 180 0,0001 350
196 110 0,0001 55
197 134 0,0001 55
198 158 0,0001 55
199 107 0,0001 55
200 131 0,0001 55
201 155 0,0001 55
202 105 0,0001 55
203 129 0,0001 55
204 153 0,0001 55
205 102 0,0001 55
206 126 0,0001 55
207 150 0,0001 55
208 178 0,0001 19
209 118 0,0001 19
210 150 0,0001 19
211 122 0,0001 19
212 133 0,0001 56
213 173 0,0001 56
214 157 0,0001 56
215 109 0,0001 56
216 132 0,0001 56
217 156 0,0001 56
```

10.2 Data output

For each time steps the solver prints a txt file with two main parts.

- Flows above all lines: end-vertexes, power flow, utilization index, centrality index.

```
[...]
117, 59, 119.7610, 14.9701, 1.2326
117, 118, 81.9942, 62.5910, 0.8439
117, 121, 21.2448, 16.2174, 0.2187
117, 178, -131.0000, 100.0000, 1.3483
118, 60, 106.5590, 13.3199, 1.0967
118, 120, 7.0432, 5.3765, 0.0725
118, 122, 60.3920, 46.1008, 0.6216
119, 61, 198.0300, 24.7538, 2.0382
119, 125, 27.6245, 21.0874, 0.2843
119, 140, -194.5224, 64.8408, 2.0021
119, 178, -45.2684, 34.5560, 0.4659
120, 62, 82.0410, 10.2551, 0.8444
120, 125, -74.9978, 57.2502, 0.7719
121, 63, 78.2690, 9.7836, 0.8056
121, 126, -57.0242, 43.5299, 0.5869
122, 64, 150.8800, 18.8600, 1.5529
122, 126, -90.4880, 69.0748, 0.9313
123, 65, 138.6210, 17.3276, 1.4267
123, 124, -18.6210, 14.2145, 0.1917
124, 66, 188.6000, 23.5750, 1.9411
124, 125, -111.3228, 84.9792, 1.1458
124, 126, -95.8982, 73.2048, 0.9870
```

```
125, 67, 191.4290, 23.9286, 1.9702
125, 127, −133.7697, 44.5899, 1.3768
125, 128, −216.3554, 72.1185, 2.2268
[...]
```

- Curtailed power at each renewable plants.

```
R, 181, −0.0000
R, 182, −0.0000
R, 183, −0.0000
R, 184, −0.0000
R, 185, 0.0000
R, 186, 0.0000
R, 187, 0.0000
R, 188, 156.4645
R, 189, −0.0000
R, 190, −0.0000
R, 191, 23.8388
R, 192, 96.1366
R, 193, 145.7316
R, 194, 264.4226
R, 195, 70.7370
R, 196, 0.0000
R, 197, 0.0000
R, 198, −0.0000
R, 199, −0.0000
R, 200, 0.0000
R, 201, −0.0000
R, 202, 0.0000
R, 203, −0.0000
R, 204, −0.0000
R, 205, 0.0000
R, 206, 0.0000
R, 207, 29.0398
```

If some storages are added into the grid, then one more txt file is provided by the solver, with as many lines as the batteries. The first number is the label of the storage node b, followed by the $SoC_{b,j}$ at the end of each time step j.

```
208 27.0 27.0 27.0 31.749983 36.499966 41.249947
    45.99993 50.749916 55.4999 50.7499 45.9999 41.2499
    36.4999 31.7499 27.0 27.0 27.0 27.0 27.0 27.0 27.0
    31.749983 36.499966 41.249947 45.99993 41.24993
    36.49993 31.749931 27.0 31.749983 36.499966
    41.249947 45.99993 41.24993 36.49993 31.749931 27.0
     31.749983 36.499966 41.249947 45.99993 50.749916
    55.4999 60.249886 64.99987 69.749855 74.49984
    79.249825 83.99981 79.24981 74.49981 69.74981
    64.99981 69.749794 74.49978 79.24976 83.99975
    88.74973 93.49972 98.2497 102.99969 98.24969
    93.49969 88.74969 83.99969 79.24969 74.49969
    69.74969 64.99969 60.249687 55.499687 50.749687
    45.999687 41.249687 36.499687 31.749687 27.0 27.0
    27.0 27.0 27.0 27.0 27.0 27.0 27.0 27.0 27.0 27.0
    27.0 27.0 27.0 27.0 27.0 27.0 27.0 27.0 27.0
```

Bibliography

[1] Application of Storage Technology for Transmission System Support: Interim Report. Technical report, EPRI, Palo Alto, CA, USA, 2012.

[2] S. Arianos, E. Bompard, A. Carbone, and F. Xue. Power grid vulnerability: A complex network approach. *Chaos: An Interdisciplinary Journal of Nonlinear Science*, 19(1):013119, 2009.

[3] L. Bam and W. Jewell. Review: power system analysis software tools. In *Power Engineering Society General Meeting, 2005. IEEE*, pages 139–144 Vol. 1, June 2005.

[4] J.P. Barton and D.G. Infield. Energy storage and its use with intermittent renewable energy. *Energy Conversion, IEEE Transactions on*, 19(2):441–448, June 2004.

[5] M. Beaudin, H. Zareipour, A. Schellenberglabe, and W. Rosehart. Energy storage for mitigating the variability of renewable electricity sources: An updated review. *Energy for Sustainable Development*, 14(4):302–314, 2010.

[6] E. Bompard, R. Napoli, and F. Xue. Extended topological approach for the assessment of structural vulnerability in transmission networks. *Generation, Transmission Distribution, IET*, 4(6):716–724, June 2010.

[7] R. Carnegie, D. Gotham, D. Nderitu, and P.V. Preckel. Utility scale energy storage systems. *State Utility Forecasting Group. Purdue University*, 1, 2013.

[8] S. Chakraborty, T. Senjyu, H. Toyama, A.Y. Saber, and T. Funabashi. Determination methodology for optimising the energy storage size for power system. *Generation, Transmission Distribution, IET*, 3(11):987–999, Nov 2009.

[9] D.P. Chassin and C. Posse. Evaluating North American electric grid reliability using the Barabási–Albert network model. *Physica A: Statistical Mechanics and its Applications*, 355(2):667–677, 2005.

[10] H. Chen, T.N. Cong, W. Yang, C. Tan, Y. Li, and Y. Dinga. Progress in electrical energy storage system: A critical review. *Progress in Natural Science*, 19:291–312, 2009.

[11] P. Crucitti, V. Latora, and M. Marchiori. A topological analysis of the Italian electric power grid. *Physica A: Statistical Mechanics and its Applications*, 338(1):92–97, 2004.

[12] A.D. Del Rosso and S.W. Eckroad. Energy Storage for Relief of Transmission Congestion. *Smart Grid, IEEE Transactions on*, 5(2):1138–1146, March 2014.

[13] B. Dunn, H. Kamath, and J.M. Tarascon. Electrical energy storage for the grid: a battery of choices. *Science*, 334(6058):928–935, 2011.

[14] K. Dvijotham, S. Backhaus, and M. Chertkov. Operations-based planning for placement and sizing of energy storage in a grid with a high penetration of renewables. *arXiv preprint arXiv:1107.1382*, 2011.

[15] A. Dwivedi, Xinghuo Y., and P. Sokolowski. Identifying vulnerable lines in a power network using complex network theory. In *Industrial Electronics, 2009. ISIE 2009. IEEE International Symposium on*, pages 18–23, Jul 2009.

[16] A. Dwivedi, Xinghuo Y., and P. Sokolowski. Analyzing power network vulnerability with maximum flow based centrality approach. In *Industrial Informatics (INDIN), 2010 8th IEEE International Conference on*, pages 336–341, Jul 2010.

[17] Eurostat. The avarage share of of electricity from renewable energy source in the Community (2004-2012). http://www.ec.europa.eu/eurostat/web/energy/data/shares, Oct 2014.

[18] L.C. Freeman, S.P. Borgatti, and D.R. White. Centrality in valued graphs: A measure of betweenness based on network flow. *Social networks*, 13(2):141–154, 1991.

[19] GNU. GLPK (GNU Linear Programming Kit). https://www.gnu.org/software/glpk/index.html.

[20] H. Ibrahim, A. Ilinca, and J. Perron. Energy storage systems: characteristics and comparisons. *Renewable and sustainable energy reviews*, 12(5):1221–1250, 2008.

[21] M. Korpaas, A. T Holen, and R. Hildrum. Operation and sizing of energy storage for wind power plants in a market system. *International Journal of Electrical Power & Energy Systems*, 25(8):599–606, 2003.

[22] A. L'Abbate, G. Migliavacca, G. Fulli, C. Vergine, and A. Sallati. The European research project REALISEGRID: Transmission planning issues and methodological approach towards the optimal development of the pan-European system. In *Power and Energy Society General Meeting, 2012 IEEE*, pages 1–8, July 2012.

[23] A. L'Abbate, G. Migliavacca, T. Pagano, and A. Vafeas. Advanced transmission technologies in Europe: A roadmap towards the smart grid evolution. In *PowerTech, 2011 IEEE Trondheim*, pages 1–8, June 2011.

[24] D. Lew, L. Bird, M. Milligan, and et al. Wind and Solar Curtailment. In *International Workshop on Large-Scale Integration of Wind Power Into Power Systems*, Sep 2013.

[25] Y.V. Makarov, Pengwei Du, M.C.W. Kintner-Meyer, Chunlian Jin, and H.F. Illian. Sizing energy storage to accommodate high penetration of variable energy resources. *Sustainable Energy, IEEE Transactions on*, 3(1):34–40, Jan 2012.

[26] G. Migliavacca, A. L'Abbate, H. Auer, and et al. Smart transmission networks in Europe: the view of REALISEGRID project. In *IFAC Proceedings Volumes (IFAC-PapersOnline)*, volume 18, pages 12867–12872, Aug 2011.

[27] F. Milano. An open source power system analysis toolbox. *Power Systems, IEEE Transactions on*, 20(3):1199–1206, Aug 2005.

[28] M. Newman. *Networks: An Introduction*. Oxford University Press, Inc., New York, NY, USA, 2010.

[29] Commission of the European Community. Limiting Global Climate Change to 2 degrees Celsius. The way ahead for 2020 and beyond , Jan 2007.

[30] H. Pandzic, Y. Wang, T. Qiu, Y. Dvorkin, and D.S. Kirschen. Near-Optimal Method for Siting and Sizing of Distributed Storage in a Transmission Network. *Power Systems, IEEE Transactions on*, PP(99):1–13, 2014.

[31] European Parliament and Council of the European Union. On conditions for access to the network for cross-border exchanges in electricity and repealing Regulation (EC) No 1228/2003. Regulation (EC) No 714/2009, Aug 2009.

[32] REALISEGRID FP7 project. http://http://realisegrid.rse-web.it/.

[33] M. Rosas-Casals, S. Valverde, and R.V. Solé. Topological vulnerability of the european power grid under errors and attacks. *International Journal of Bifurcation and Chaos*, 17(07):2465–2475, 2007.

[34] P.M. Subcommittee. IEEE reliability test system. *Power Apparatus and Systems, IEEE Transactions on*, PAS-98(6):2047–2054, Nov 1979.

[35] A. Sullivan and S.M. Sheffrin. *Economics: Principles in action*. 2003.

[36] Electrical Energy Storage Project Team. Electrical energy storage. Technical report, IEC, 2009.

[37] Terna. Dati "Terna" 2010. http://www.terna.it/default/Home/SISTEMA_ELETTRICO/statistiche/dati_statistici.aspx.

[38] Terna. Dati "Terna" 2012. http://www.terna.it/default/Home/SISTEMA_ELETTRICO/statistiche/dati_statistici.aspx.

[39] Terna. Statistical data on electricity in Italy 2012. http://www.terna.it/default/home_en/electric_system/statistical_data.aspx.

[40] A. C. Tortora, E. Senatore, L. Apicella, and R. Polito. Sistemi di accumulo di energia elettrochimici per la gestione efficiente delle fonti rinnovabili non programmabili. *L'Energia Elettrica*, 91(4):35–46, Jul/Aug 2014.

[41] E. Vineti. Strumenti di ottimizzazzione per le reti elettriche. Bachelor's thesis, Universita' di Modena, 2015.

[42] X.Y. Wang, D. Mahinda Vilathgamuwa, and S.S. Choi. Determination of battery storage capacity in energy buffer for wind farm. *Energy Conversion, IEEE Transactions on*, 23(3):868–878, Sept 2008.

[43] P. Wong, P. Albrecht, R. Allan, and et al. The IEEE Reliability Test System-1996. A report prepared by the Reliability Test System Task Force of the Application of Probability Methods Subcommittee. *Power Systems, IEEE Transactions on*, 14(3):1010–1020, Aug 1999.